This is the peer reviewd version of the followng article:

Classification of EEG abnormalities in partial epilepsy with simultaneous EEG-fMRI recordings / Pedreira, C.; Vaudano, Anna Elisabetta; Thornton, R. C.; Chaudhary, U. J.; Vulliemoz, S.; Laufs, H.; Rodionov, R.; Carmichael, D. W.; Lhatoo, S. D.; Guye, M.; Quian Quiroga, R.; Lemieux, L.. - In: NEUROIMAGE. - ISSN 1053-8119. - 99:(2014), pp. 461-476. [10.1016/j.neuroimage.2014.05.009]

Terms of use:

The terms and conditions for the reuse of this version of the manuscript are specified in the publishing policy. For all terms of use and more information see the publisher's website.

19/04/2024 23:51

(Article begins on next page)

NeuroImage xxx (2014) xxx–xxx

Contents lists available at ScienceDirect

NeuroImage

journal homepage: www.elsevier.com/locate/ynimg

Classification of EEG abnormalities in partial epilepsy with simultaneous EEG–fMRI recordings

C. Pedreira [a,1], A.E. Vaudano [b,c,1], R.C. Thornton [c], U.J. Chaudhary [c], S. Vulliemoz [d], H. Laufs [e], R. Rodionov [c], D.W. Carmichael [c,f], S.D. Lhatoo [g], M. Guye [h,i], R. Quian Quiroga [a,j], L. Lemieux [c,*]

[a] Centre for Systems Neuroscience, The University of Leicester, UK
[b] Department of Neuroscience, NOCSAE Hospital, University of Modena e Reggio Emilia, Modena, Italy
[c] Department of Clinical and Experimental Epilepsy, UCL Institute of Neurology, London, UK
[d] Department of Neurology, University Hospital of Geneva, CH-1211 Genèva 14, Switzerland
[e] Department of Neurology, Schleswig Holstein University Hospital, Kiel, Germany
[f] Imaging and Biophysics Unit, UCL Institute of Child Health, London, UK
[g] Division of Medical Informatics, Case Western Reserve University, Cleveland, OH, USA
[h] Aix-Marseille Université, CNRS, CRMBM UMR 7339, Marseille, France
[i] APHM, Hôpitaux de la Timone, Service de Neurophysiologie Clinique & CEMEREM, Marseille, France
[j] Leibniz Institute for Neurobiology, Magdeburg, Germany

ARTICLE INFO

Article history:
Accepted 2 May 2014
Available online xxxx

Keywords:
IED
EEG–fMRI
Automatic classification
Focal epilepsy
icEEG

ABSTRACT

Scalp EEG recordings and the classification of interictal epileptiform discharges (IED) in patients with epilepsy provide valuable information about the epileptogenic network, particularly by defining the boundaries of the "irritative zone" (IZ), and hence are helpful during pre-surgical evaluation of patients with severe refractory epilepsies. The current detection and classification of epileptiform signals essentially rely on expert observers. This is a very time-consuming procedure, which also leads to inter-observer variability. Here, we propose a novel approach to automatically classify epileptic activity and show how this method provides critical and reliable information related to the IZ localization beyond the one provided by previous approaches. We applied *Wave_clus*, an automatic spike sorting algorithm, for the classification of IED visually identified from pre-surgical simultaneous Electroencephalogram–functional Magnetic Resonance Imagining (EEG–fMRI) recordings in 8 patients affected by refractory partial epilepsy candidate for surgery. For each patient, two fMRI analyses were performed: one based on the visual classification and one based on the algorithmic sorting. This novel approach successfully identified a total of 29 IED classes (compared to 26 for visual identification). The general concordance between methods was good, providing a full match of EEG patterns in 2 cases, additional EEG information in 2 other cases and, in general, covering EEG patterns of the same areas as expert classification in 7 of the 8 cases. Most notably, evaluation of the method with EEG–fMRI data analysis showed hemodynamic maps related to the majority of IED classes representing improved performance than the visual IED classification-based analysis (72% versus 50%). Furthermore, the IED-related BOLD changes revealed by using the algorithm were localized within the presumed IZ for a larger number of IED classes (9) in a greater number of patients than the expert classification (7 and 5, respectively). In contrast, in only one case presented the new algorithm resulted in fewer classes and activation areas. We propose that the use of automated spike sorting algorithms to classify IED provides an efficient tool for mapping IED-related fMRI changes and increases the EEG–fMRI clinical value for the pre-surgical assessment of patients with severe epilepsy.

© 2014 Published by Elsevier Inc.

Introduction

Non-invasive techniques for recording brain activity are widely used to assess neurological conditions and improve the understanding of healthy brain function (Emerson and Pedley, 2000). In patients affected by epilepsy, scalp Electroencephalography (EEG) recordings represent a fundamental tool for identifying pathological brain activity and hence support epileptic syndrome diagnosis (Hogan, 2011). Interictal epileptiform discharges (IED; commonly referred to as 'epileptic spikes') are seen in recordings from patients with focal and generalised epilepsies and their recognition and classification provide information about the mechanisms of ictiogenesis (Ebersole, 1997). Furthermore, experimental studies have suggested that interictal spikes might precede the

* Corresponding author at: MRI Unit, National Society for Epilepsy, Chesham, Lane, Chalfont St Peter, Buckinghamshire SL9 0RJ, UK. Fax: +44 1494 875 666.
E-mail address: louis.lemieux@ucl.ac.uk (L. Lemieux).
[1] Equal contribution.

http://dx.doi.org/10.1016/j.neuroimage.2014.05.009
1053-8119/© 2014 Published by Elsevier Inc.

Please cite this article as: Pedreira, C., et al., Classification of EEG abnormalities in partial epilepsy with simultaneous EEG–fMRI recordings, NeuroImage (2014), http://dx.doi.org/10.1016/j.neuroimage.2014.05.009

UNCORRECTED PROOF

ARTICLE IN PRESS

occurrence of spontaneous seizures and might contribute to the development and maintenance of the epileptic state (Staley et al., 2011; White et al., 2010). Finally, IED and their topographic distributions define the boundaries of the "irritative zone" (IZ; area from which IED arise) and hence can be used during the pre-surgical evaluation of patients with severe drug-resistant epilepsy (Luders, 1993).

Simultaneous recording of EEG and functional MRI (EEG–fMRI) is a technique capable of revealing the brain regions hemodynamically involved by the epileptic discharge based on local blood oxygenation level dependent (BOLD) signal variations. In patients with refractory focal epilepsy the significant clinical question is how the EEG–fMRI results can contribute to localize the seizure onset zone (SOZ), the brain region that is thought to be responsible for generating seizures. To date, the intracranial EEG recordings (icEEG) are considered the gold standard for identifying the SOZ (Rosenow and Luders, 2001), although it is expensive and has associated morbidity (Hamer et al., 2002). There has been great effort in the study of IED, which are generally much more abundant than ictal events, as marker of the SOZ by non-invasive means; in particular there have been attempts to identify whether a specific type of IED is a specific marker of the SOZ (or epileptogenic zone). This is one of the motivations for performing EEG–fMRI of IED by the study of the associated BOLD patterns (Pittau et al., 2012; Thornton et al., 2010, 2011). More importantly, it has been demonstrated that when the surgical resection completely removed the region in which IED correlated BOLD signal change, it is associated with a better outcome and seizure freedom (Thornton et al., 2010). Similar conclusions have been reached by using the Electrical Source Imaging (ESI) approach on high-density scalp EEG during the pre-surgical evaluation protocol (Mégevand et al., 2013). This evidence further supports the importance of a correct definition of IED generators in order to improve surgery outcome. However, caution must be required in extrapolating the results of any interictal investigation to make inferences about the epileptogenic zone. The definition of the irritative zone is indeed an important aspect in the evaluation of the SOZ, but not equivalent to it (Dworetzky and Reinsberger, 2011).

In routine clinical practice, the detection and classification of IED continue to be based on visual inspection by expert observers using waveform morphology and field distribution. Similarly, the modelling of epileptic activity-related hemodynamic changes using fMRI relies mostly on visual identification, classification and marking of the epileptic EEG patterns (Al-Asmi et al., 2003; Salek-Haddadi et al., 2006). The detection and classification of IEDs can be a time-consuming procedure, especially in the case of (continuous) long-term EEG monitoring (Ramabhadran et al., 1999) and requires experienced reviewers for visual identification and quantification of epileptic discharges (Scherg et al., 2012). Additionally, the subjectivity and poor reproducibility of IED detection and classification are well documented (Hostetler et al., 1992; Webber et al., 1993). In the EEG–fMRI studies the presence of artefacts on the EEG, caused by electromagnetic gradients and physiological noise, may indeed alter the quality of the recordings and hence influence the IED identification (Siniatchkin et al., 2007). The inaccurate or inconsistent labelling of IEDs in simultaneous EEG–fMRI recordings was shown to be an important source of error on the related hemodynamic maps (Flanagan et al., 2009). Particularly, a linear correlation between the proportions of IED included in the analysis and the percentage of voxels within the fMRI maps above a significant statistical threshold has been shown (Flanagan et al., 2009). Correct IED identification and classification clearly reduce the percentage of false positive and false negative BOLD results improving the scientific and clinical interpretation of the results of fMRI studies in epileptic patients, especially in those cases where a correct localization of the SOZ and IZ is crucial for patients' management as refractory epilepsies candidate for surgery. Furthermore, quantitative approaches to EEG interpretation for the purpose of mapping epileptic hemodynamic changes can lead to significantly increased sensitivity (Grouiller et al., 2011; Liston et al., 2006; Vulliemoz et al., 2011).

Here, we propose a pilot study presenting a novel approach to the problem of IED classification for posterior analysis in scalp EEG recordings with synchronous fMRI: the use of *Wave_clus* (Quian Quiroga et al., 2004), a spike sorting algorithm, for the classification of the visually identified events. This algorithm exploits the statistical properties of the IEDs (in contrast to random variance due to noise in the recorded signal) to identify the intrinsic characteristic of each class. We hypothesize that this analysis can provide additional information regarding the identification of IZ and the epileptic network, providing further clinical insight valuable for diagnosis and hence subsequent surgical treatment when indicated. We also assess the performance of the automatic IED classification by estimating the level of agreement with the results of expert classification, based on the fMRI data analysis findings obtained for both methods.

Materials and methods

Patients

76 patients with refractory partial epilepsy were recruited as part of an EEG–fMRI study at University College London (Thornton et al., 2010). The patients were undergoing pre-surgical evaluation at three centres: National Hospital for Neurology and Neurosurgery, London, UK; Frenchay Hospital, North Bristol NHS Trust, UK; and Hopital la Timone, Marseille, France, to identify the SOZ and IZ, included a detailed clinical history, full neurological examination, Video-EEG telemetry, structural MRI scanning, neuropsychological assessment and other non-invasive investigations such as PET, MEG and ictal SPECT when available. The definition of the IZ is based on the Video-EEG monitoring and MEG when available (Rosenow and Luders, 2001). icEEG recordings were considered based on the availability of hypotheses derived from spatial localization of ictal and interictal discharges recorded non-invasively. In patients who underwent icEEG, this was used to define the IZ and SOZ; in the other patients they were defined (qualified as 'presumed') based on the Video-EEG monitoring and MEG when available (Rosenow and Luders, 2001). The EEG–fMRI recordings took place at University College London. In this article we report on the 8/76 patients in whom at least 200 IED were recorded during the EEG–fMRI session (6 males, age range: 19–41 years, mean: 27 years).

All procedures were subject to local Research and development directorate guidelines in addition to National Research Ethics Committee Approval in the UK and France.

EEG–fMRI acquisition

The patients were asked to remain still during the scanning, fitted with ear-plugs, with their head immobilized using a vacuum cushion. 32 or 64 EEG channels were recorded at a sampling rate of 5000 Hz using a commercial MR-compatible system (BrainAmp MR and Vision Analyzer, Brain Products GMbH, Munich, Germany); the ECG was recorded using a single lead (Allen et al., 1998; Vulliemoz et al., 2011). EEG was recorded for 5–20 min with eyes closed outside the scanner immediately prior to scanning. At least two 20-minute sessions of resting-state EEG–fMRI were acquired separated by a short break. A third 20-minute session was recorded in some patients if tolerated. Each session consisted of 404 T2*-weighted single-shot gradient-echo echo-planar images (EPI; TE/TR 30/3000 ms, flip angle 90: 43 2.5 mm interleaved slices, FOV: 24 × 24cm^2, matrix: 64 × 64) acquired continuously on a 3 Tesla Signa Excite HDX MRI scanner (General Electric, Milwaukee, WI, USA). A 5-minute finger tap task was also recorded during fMRI for each case. T1-weighted MRI scans were also acquired at the same time (imaging parameters: TE = 3.1 ms, TR = 8.3 ms, inversion time = 450 ms, flip angle = 20°, slices = 170, slice thickness = 1.1 mm, filed of view = 24 × 18 and matrix = 256 × 256 cm^2) to allow accurate anatomical localization of BOLD signal changes.

UNCORRECTED PROOF

Please cite this article as: Pedreira, C., et al., Classification of EEG abnormalities in partial epilepsy with simultaneous EEG–fMRI recordings, NeuroImage (2014), http://dx.doi.org/10.1016/j.neuroimage.2014.05.009

EEG pre-processing and analysis

EEG artefacts induced by the MR scanning gradients and heartbeats were corrected (Allen et al., 1998, 2000) using a commercial EEG processing package (Brain Analyzer; Brain Products). For each EEG recording, IED were identified, marked and labelled by an expert (AEV, SV, UC or RT) to reflect distinct generators based on IED morphology and field distribution.

IED sorting and classification

Spike sorting algorithms are typically used for the analyses of extracellular recordings (Quian Quiroga, 2007). Advances in electrode designs have proven that these algorithms are especially effective for extracting information from multiple site recordings, resulting in high quality classification of signal sources (Blanche et al., 2005; Gray et al., 1995).

The solution to the problem of classifying multichannel scalp EEG events presented here is based on *Wave_clus*, a spike sorting algorithm that performs a wavelet decomposition of the signals in combination with superparamagnetic clustering, a clustering method from statistical mechanics (Quian Quiroga et al., 2004). This combination allows identifying small but consistent differences in the analysed signals. Furthermore, the superparamagnetic clustering algorithm does not assume any a priori number of classes or cluster shape in the feature space. Therefore, *Wave_clus* is an ideal candidate for the analysis of IED and their classification according to the waveforms provided by different electrodes.

Fig. 1 shows a summary of the steps followed for IED processing in a representative case (#7). For the automated processing of the IED we band passed the recorded signals. We heuristically explored a range of low cut frequencies the recorded signals between 0.5 and 10 Hz, reaching best performance at 4 and high cut frequency of 50 Hz using an 8 order elliptic band pass filter. Next, we selected a subset of between 8 and 12 most active channels for each patient based on the clinical evidence (Fig. 1A). EEG channel selections are described in Table 1. Next, for each IED visually identified by the expert a window of 300 ms around the marked time (from 80 ms pre-peak to 220 ms post-peak) was used for processing each of the channels selected. To provide robustness against possible jitter sources for each event in the signal of different channels, the IED were aligned at their negative peak found within a 40 ms window centred at the time of the channel presenting larger amplitude of the IED. For each IED, the signals from the selected channels were then concatenated to form what we call a 'meta-IED' (Fig. 1B).

Each dataset (2 or 3 EEG–fMRI sessions), consisting of all the meta-IED for a given patient's recording, was then analysed with *Wave_clus* independently from the expert classification. First, the algorithm performed a wavelet transform of the meta-IED using Haar wavelets, which are ideal to capture small variations in the signal. Then, the coefficients obtained were tested for multimodality to distinguish between the variances due to noise (supposing this is normally distributed) and the ones reflecting two or more consistent values (multimodal distributions), using a Kolmogorov–Smirnov test (see Quian Quiroga et al., 2004 for details), thus providing coefficients that potentially separate the spikes into different clusters. In our case we selected a total number of coefficients equal to 8 times the number of channels of the meta-IED data (i.e. 8 wavelet coefficients per 75 data points). The obtained coefficients were then introduced in the superparamagnetic

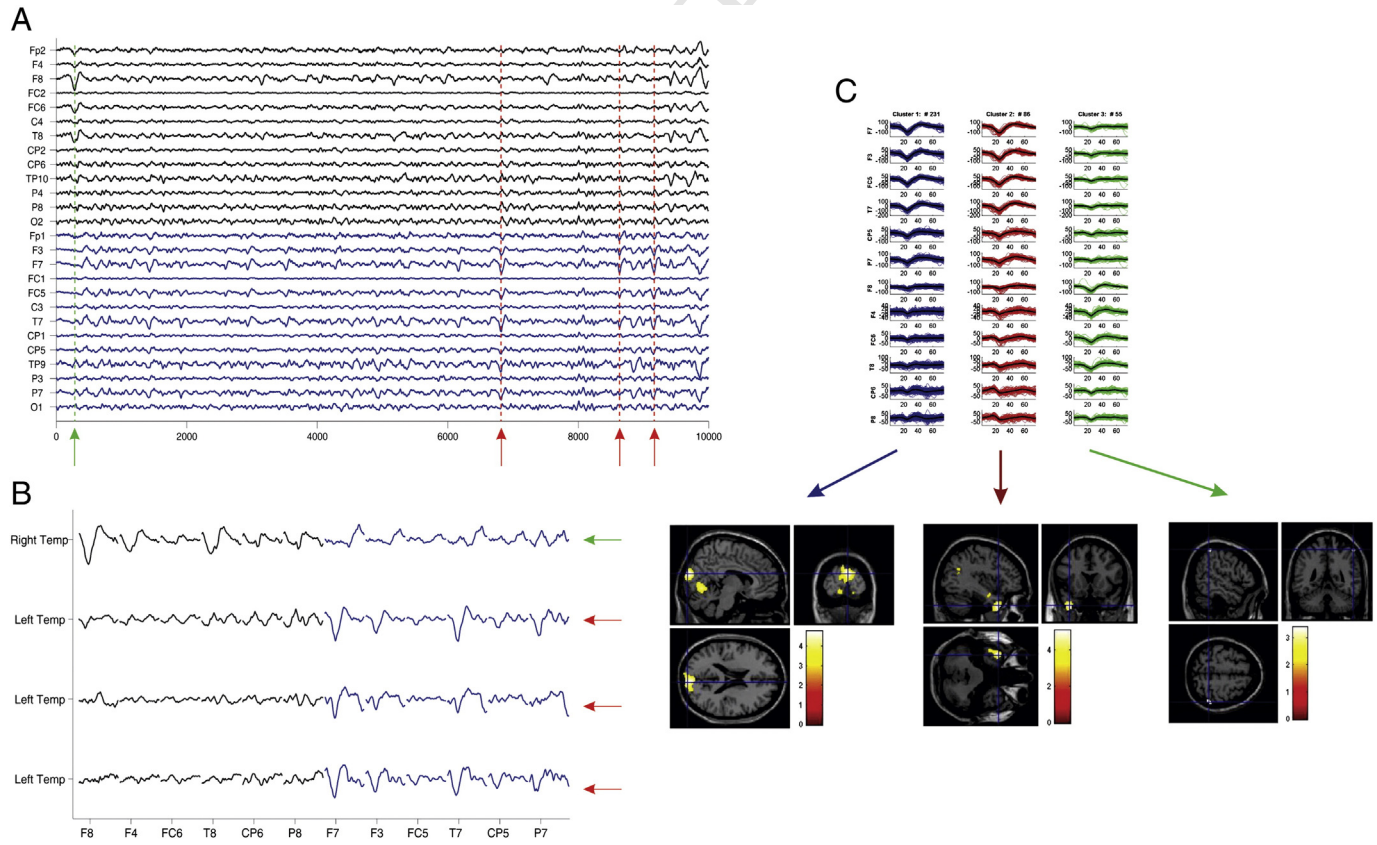

Fig. 1. Summary of cluster sorting process for EEG recordings with *Wave_clus*, example from case #7. Panel A: The continuous signal was filtered and the events marked by the expert. In the example, the green arrow indicates a right temporal event and the red arrows the left temporal events. Panel B: Composition of the meta-IED using the selected channels based on clinical criteria. Panel C: Clusters obtained with *Wave_clus* and associated fMRI maps. For Class 1 there was a cluster of BOLD signal increase over the bilateral cuneus and the mesial occipital cortex (left). Class 2 presented a cluster of activation in the left temporal pole (middle). Class 3 presented a cluster of activation in the right parietal lobe, BA40 (right). Results are displayed on the canonical T1-weighted image ($p < 0.001$ uncorrected for FWE). R = right; L = left.

Please cite this article as: Pedreira, C., et al., Classification of EEG abnormalities in partial epilepsy with simultaneous EEG–fMRI recordings, NeuroImage (2014), http://dx.doi.org/10.1016/j.neuroimage.2014.05.009

Table 1
IED classification results.

Case	Epilepsy syndrome and localisation	Visual IED classification/n°of IED	EEG channels selection	Wave_clus IED classification/no of IED
#1	R TLE	IED1. L T/666	F8, T8, FC6, CP6, FT8, T7, P7, CP5, TP9, TP7	C1. Low amplitude L FT/390
		IED2. R T/468		C2. Low amplitude R FT/210
				C3. High amplitude L FCT/127
				C4. Low amplitude B O Slow wave/149
				C5. High amplitude L TP spikes with R FT diffusion/84
				C6. High amplitude B FT(>L)/85
				C7. High amplitude R FCT/89
#2	R FLE	IED1. R F/2260	Fp2, F4, F8, P8, O2, Fp1, P7, O1	C1. High amplitude R F/1329
				C2. Low amplitude diffuse/378
				C3. High amplitude diffuse/553
#3	R FLE	IED1. B F (>R)/253	Fp2, F4, FC6, T8, CP6, P8, Fp1, F3, FC5, T7, CP5	C1. Low amplitude B FC (>R)/227
		IED2. R F/71		C2. Low amplitude L FT/20
		IED3. L T/21		C3. High amplitude diffuse (>CT)/58
		IED4. L F/18		C4. Low amplitude diffuse/61
		IED5. R T/2		
#4	L PLE	IED1. L P Sh-W/139	F4, C4, P4, FC2, CP2, F3, C3, P3, FC1, CP1	C1. High amplitude L CPT/187
		IED2. L P/94		C2. Low amplitude L CPT/56
		IED3. L P-T/20		C3. High amplitude L CP/23
		IED4. L P PP/12		
#5	L FLE	IED1. L F/114	Fp2, F4, F8, T8, P8, Fp1, F3, F7, T7, P7	C1. Low amplitude diffuse/138
		IED2. L F Sh-W/74		C2. Low amplitude B F(>L)/67
		IED3. L F PP/64		C3. High amplitude diffuse(>F)/127
		IED4. L F ant/60		C4. Low amplitude L F/44
		IED5. L F inf/38		
		IED6. L F SW/19		
		IED7. L F Sh-Th/3		
#6	L TLE	IED1. L T/225	Fp1, F7, F3, FC5, T7, C3, FC5, P7, P3, O1	C1. High amplitude L Hemisphere (>T)/186
				C2. Medium amplitude L Hemisphere (>CT)/39
#7	L OLE	IED1. L T/311	F7, F3, FC5, T7, CP5, P7, F8, F4, FC6, T8, CP6, P8	C1. High amplitude L FT/231
		IED2. R T/60		C2. High amplitude L FT with diffusion to R CP/86
		IED3. B T/1		C3. Low amplitude R T/55
#8	R PLE	IED1. Midline Cz/206	Fp1, AF3, FC1, CP1, Fp2, AF4, FC2, CP2	C1. Low amplitude B FCP/210
		IED2. R FC/121		C2. High amplitude B FC/60
		IED3. R F/10		C3. Low amplitude B F(>r)/67

Legend Table 1: IED: Interictal Epileptic Discharges; C: Classes according to *Wave_clus*; L: left; R: right; B: bilateral; F: Frontal; T:Temporal; P: Parietal; O:Occipital; PT: Parieto-Temporal; FC: Fronto-Central; CT: centro-temporal; FCP: fronto-centro-.parietal; FCT: fronto-centro-.temporal; sup: superior; ant: anterior; inf:inferior; post: posterior; Sh-W: Sharp-Waves; PP: polyspikes; SW: Spike-Waves; inf: inferior; ant: anterior; Sh-Th: Sharp-Theta. See text for details. The black colour underlining identifies the IED classes (for both visual and automatic labelling) more clinically relevant.

clustering algorithm, obtaining the proposed automatic classification of IEDs. When the automatic solution was not fully satisfactory the user could use the provided interface to merge or reject the automatically obtained clusters candidates to reach a better solution. This process was performed with the results of the manual classification hidden from the user performing the clustering. The upper part of Fig. 1C shows the 3 classes obtained from the selected channels. We then obtained the fMRI localization of each class, as shown in the bottom of Fig. 1C.

After classification, we computed the mean (over 1 s) of the signal across all EEG channels for each class. We then labelled the *Wave_clus* classes based on the scalp localization and amplitude of the events. In section S1 of the Supplementary Material the level of agreement between the non-invasive defined IZ localization and IED type is quantified for both classification methods.

In addition, we compared the visual-based classification with the automatic approach in terms of number of IED classes and their topographic distribution on the scalp (see Supplementary Material S1).

fMRI data analysis

In order to map BOLD changes related to the IEDs, we analysed fMRI data within the General Linear Model (GLM) framework.

For each patient, two fMRI models were employed, one correlated to IED as classified visually (GLM1), the second using IED classes labelled using *Wave_clus* (GLM2). All fMRI data were pre-processed and analysed using SPM8 (http://www.fil.ion.ucl.ac.uk/spm/). After discarding the first four image volumes (T1 saturation effects), the EPI time series were realigned, and spatially smoothed with a cubic Gaussian Kernel of 8 mm full width at half maximum. fMRI time-series data were then analysed to determine the presence of regional IED-related BOLD changes. Motion-related effects were modelled in the GLM by 24 regressors derived from the 6 scan realignment parameters (Friston et al., 1996). An additional set of confounds was included to account for large head movements (Lemieux et al., 2007) and cardiac-related signal changes (Liston et al., 2006). The stick functions representing the IED onsets were convolved with the canonical hemodynamic response function (HRF) plus its temporal and dispersion derivatives testing for IED-related BOLD signal changes.

Two T contrasts were specified to test for significant IED-related BOLD increases and decreases respectively; the resulting SPM were thresholded at $p < 0.001$ (uncorrected for multiple comparisons) with an additional extent threshold of five voxels. In cases where no significant change was related for T contrasts over the individual IED types, we used an F contrast across all IED types to assess the presence of BOLD change related to any linear combination of the various IED classes. The results were overlaid onto the subject's structural MRI (T1 image) or mean EPI for illustration purposes.

Comparison of the EEG–fMRI results with electro-clinical information and intracranial EEG recordings

To test our main hypothesis, the BOLD maps resulting from the two GLMs were compared for each IED class. More specifically, the following BOLD map features were considered for the comparison: 1) the BOLD cluster containing the statistically most significant change (global

Please cite this article as: Pedreira, C., et al., Classification of EEG abnormalities in partial epilepsy with simultaneous EEG–fMRI recordings, NeuroImage (2014), http://dx.doi.org/10.1016/j.neuroimage.2014.05.009

maximum: GM); 2) other, less significant, BOLD clusters, except those located in the ventricular system, vascular tree and confined to the edges of the brain. For patients who underwent invasive EEG recording during the pre-surgical workout, we compared the BOLD maps with the invasively-defined IZ. For patients who did not undergo icEEG, we compared the BOLD maps with the presumed IZ, which was defined at the lobar level on the basis of non-invasive electro-clinical information (epileptiform discharges recorded on clinical long term video EEG recordings, seizures semiology, radiological findings, PET and ictal SPECT if available) (Pittau et al., 2012).

For both subgroups of patients, the degree of concordance of the EEG–fMRI results with the IZ was determined by visual inspection of the SPM for each IED class. Following our previous work (Chaudhary et al., 2012), for each IED class, the level of concordance of the positive and negative BOLD maps was classified in the following categories:

- Concordant [C]: all BOLD clusters within the IZ (within 2 cm around the IZ and in the same lobe).
- Concordant plus [C+]: GM BOLD cluster within the IZ (within 2 cm around the IZ in the same lobe), and at least one cluster remote from the IZ.
- Discordant plus [D+]: GM BOLD cluster remote from the IZ and at least one cluster in the IZ (within 2 cm around the IZ in the same lobe).
- Discordant [D]: all clusters remote from the IZ.
- Null [N]: no significant clusters.

In addition, the algorithm-derived fMRI maps were compared to check for over-classification of IED. A sign of over-classification would be (practically) identical maps for different IED classes. This was noted if present, on the basis of the fMRI results only, without considering the expert's visual IED classification.

Results

Table 2 summarises the clinical data obtained using conventional assessment methods. Structural MRI scans revealed right frontal atrophy without any clear focal lesion in one patient (#2), FCD in 3 patients (#4, #7 and #8) and no anatomical abnormality in the rest. Four out of eight patients subsequently underwent icEEG (#2, #4, #7 and #8). In one subject icEEG was not performed due to seizure onsets at several discrete sites. In all cases there was good correspondence between SOZ and IZ. For the four patients in whom surgery was performed, surgical outcome at 12 months post-operatively was assessed: three patients (#4, #7, #8) were seizure-free after resection (ILAE 1) and in the other (#2) there was a poor outcome (ILAE 5).

IED classification

The average number of IED identified per patient during EEG–fMRI was 411 events (range: 225–2260). Table 1 describes the IED classifications for the two methods for each patient. The most clinically relevant IED classes (in terms of concordance with the clinical hypothesis, not considering invasive procedures) for both classification methods are underlined in the table. In the Supplementary Material S1 we provide a more detailed description and comparison of the topographical results for both classification methods. Additionally, Supplementary Fig. S1 illustrates the algorithmic classification results and plots of the mean IED waveform for each class and Supplementary Figs. S2–S9 show the topographic distribution of amplitudes for each class at the time of the spike peak.

Visual IED classification

Across all subjects a total of 26 IED types were visually identified. There was a single IED type identified in 2 patients (#2 and #6), and two or more IED types in the other cases (#1, #3, #4, #5, #7 and #8). The differentiating IED feature was related to localization in 4 patients (patients #1, #3, #7 and #8), morphology in one (#5) and a combination of both in another (#4).

Algorithmic (Wave_Clus) IED classification

A total of 29 IED classes were identified by the automatic approach across the group; for each subject at least two (#6) or more (#1, #2, #3, #4, #5, #7 and #8) IED types were found. The differentiating IED trait was related to localization in 3 patients (patients #1, #7 and #8), spike amplitude in one (#6) and a combination of both in the remaining (#2, #3, #4 and #5).

IED-related BOLD changes

We compared the EEG–fMRI results for the models derived from the visual (GLM1) and the algorithmic (GLM2) IED classifications. Table 3 summarises the EEG–fMRI results for the two IED classifications. In the following, we describe the BOLD changes for all cases, followed by a comparison of the GLM2 and GLM1 results.

Comparison of interictal BOLD changes with the invasively–defined IZ

In the four patients (#2, #4, #7, #8) who underwent icEEG recordings, the structural MRI scan revealed brain abnormalities in all of them.

GLM1. The BOLD global maximum was located within the IZ (concordance classified as C or C+) related to one type of visually labelled

CORRECTED PROOF

Table 2
Patients' electro-clinical details.

PT	Epilepsy syndrome	Gender/age	IEDs	Ictal EEG	Structural MRI	Intracranial EEG	Surgical outcome at 12 months
#1	R TLE	M/24 years	Independent R FT, mid-T, Spikes; L T spikes	R hemisphere onset, probably multifocal	Normal	N/A (Multifocality)	N/A
#2	R FLE	M/25 years	Bi-F spike wave discharge. (Max: F4-C4)	Continuous bi-F rhythmic spike-wave discharges max F4-C4	R F atrophy	SOZ = IZ: R pre-F cortex, ACC, mesial SMA	Class 5
#3	R FLE	M/25 years	SWD 3–4hz, anterior predominant R > L	fast activity over right hemisphere	Normal	Awaiting	N/A
#4	L PLE:	F/29 years	L P and L PT sharp waves and slow wave	LP fast activity with spread to anterior leads	FCD over L angular gyrus	SOZ = IZ: L angular gyrus	Class 1
#5	L FLE	F/41 year	L F (F3) Spikes, Bilat SWD (LF emphasis)	bifrontal theta, bilat SWD	Normal	Declined	N/A
#6	L TLE	M/19 years	L T Spikes	L T rhytmic theta	Normal	Declined	N/A
#7	L OLE	M/24 years	L mid-post sharp-waves (max T3-T5)	Left posterior TP;	L O FCD	SOZ = L medial OL IZ = L OL, R OL, L medial PL	Class 1
#8	R PLE	M/31 year	RP and R central spikes	Not specific	R P FCD	SOZ = IZ: R pericentral cortex	Class1 (5 months)

Legend: R = right, L = left, IZ = irritative zone, SOZ = ictal onset zone, T = Temporal, F = Frontal, O = Occipital, P = Parietal, TLE = temporal lobe epilepsy, PLE = parietal lobe epilepsy, FLE = frontal lobe epilepsy, Inf = inferior, Sup = superior, EEG = electroencephalogram, FCD = Focal cortical dysplasia, ACC = anterior cingulate cortex, SMA = supplementary motor area, N/A = not available, SWD = spike-wave discharges, M = male, F = female, FCD = focal cortical dysplasia, OL: occipital lobe, PL: parietal lobe.

Please cite this article as: Pedreira, C., et al., Classification of EEG abnormalities in partial epilepsy with simultaneous EEG–fMRI recordings, NeuroImage (2014), http://dx.doi.org/10.1016/j.neuroimage.2014.05.009

ARTICLE IN PRESS

Table 3
fMRI data analysis results.

Case	Clinical IZ localization	FMRI results (visual IED classification)							FMRI results (*Wave_clus* IED classification)					
		BOLD Signal Changes (sign of peak change)	Level of concordance						BOLD signal changes (sign of peak change)	Level of concordance				
			C	C+	D+	D	N			C	C+	D+	D	N
#1	Uncertain, probably R T lateralized	IED1: B TL mid-post (d)*(GM)* + L TL pole (i)			▪				C1. R SMA(i)*(GM)* + R sup F gyrus(i/d)				▪	
		IED2: R post cingulate (d)*(GM)*				▪			C2.					▪
									C3. L TL mid-post(d) *(GM)* + L TL pole(i)			▪		
									C4.					▪
									C5.					▪
									C6.					▪
									C7. R middle T gyrus(i)*(GM)*	▪				
#2	SOZ = IZ: R pre-F cortex, ACC, mesial SMA	IED1: DMN(d)*(GM)* + R ACC(i) + R sup T gyrus(i) + R Medial F gyrus(i) + R SMA(BA6) (i) + Brainstem(d)			▪				C1. R orbitofrontal(i)*(GM)* + ACC(i) + R SMA(i) + R prefrontal (i) + DMN(d) + Brainstem(d) + BG(d)		▪			
									C2.					▪
									C3. R sup T gyrus*(GM)* (i) + R orbito-frontal(i) + DMN(d) + Brainstem(d) + BG(d)			▪		
#3	Uncertain, probably R F lateralized	IED1: B Sup F Gyrus (>R)(i)*(GM)* + L perisylvian (i) + Posterior DMN (d)		▪					C1. B cerebellum (>L) (i/d)*(GM)* + R Sup F gyrus(i) + post T cortex(i) + L perisylvian(d)			▪		
		IED2: L cerebellum (GM)				▪			C2.					▪
		IED3					▪		C3-C4. B perisylvian(i)*(GM)* + L medial F gyrus(i) + R PC(i) + L precentral F(i)			▪		
		IED4					▪							
		IED5					▪							
#4	SOZ = IZ: L angular gyrus	IED1: L PL (i)*(GM)*	▪						C1. B PL(>L)(i)*(GM)* + L cerebellum(d)		▪			
		IED2					▪		C2 L medial F gyrus(i) *(GM)* + L orbitofrontal cortex + B (>L) T pole(i)				▪	
		IED3: L medial F gyrus (i) *(GM)*				▪			C3. R orbitofrontal cortex(GM) + B(>L) medial F gyrus(i) + B T (>R) pole(i) + B O cortex				▪	
		IED4: L precentral cortex (i)*(GM)*				▪								
#5	Uncertain, probably LF lateralized	(IED1 + 2 + 3 + 4*): L Sup F Gyrus (i)*(GM)*	▪						C1-C4. L Sup F Gyrus(i)*(GM)*	▪				
		IED5					▪		C2.					▪
		IED6					▪		C3.					▪
		IED7					▪							
#6	Uncertain, probably L T lateralized	IED1: Pc(d)*(GM)* + L F precentral(i) + B TL(d)				▪			C1. L F precentral(i)*(GM)* + B TL(d) + Pc(d)				▪	
									C2. L T pole(i) + Post TL (i)*(GM)*		▪			
#7	IZ = L OL, R OL, L medial PL	IED1: B Mesial O cortex (i) *(GM)* + L O Pole (i)		▪					C1. B Mesial O cortex(i)*(GM)* + B cuneus + brainstem(d)		▪			
		IED2					▪		C2. L T pole(i)*(GM)*				▪	
		IED3					▪		C3. R P lobe(i)*(GM)*				▪	
#8	SOZ = IZ: R pericentral cortex	IED1: R Middle F gyrus (i) *(GM)*				▪			C1. R Medial F gyrus(i)*(GM)*	▪				
		IED2: R Medial F gyrus (i) *(GM)*	▪						C2. R Middle F gyrus(i)*(GM)*				▪	
		IED3					▪		C3. L Prefrontal cortex(i)*(GM)*				▪	

Legend table 3 IED: Interictal Epileptic discharges; L: left; R: right; SOZ: Seizure Onset Zone; IZ: Irritative Zone; B: bilateral; F: Frontal; T:Temporal; P: Parietal; O:Occipital; PT: Parieto-Temporal; FC: Fronto-Central; sup: superior; ant: anterior; inf:inferior; post: posterior; Sh-W: Sharp-Waves; PP: polyspikes; SW: Spike-Waves; inf: inferior; ant: anterior; Sh-Th: Sharp-Theta. ACC = Anterior Cingulate Cortex ; SMA: Supplementary Motor Area; BG: basal Ganglia; Pc: precuneus; th: thalamus; DMN: Default Mode Network; TLE Temporal Lobe Epilepsy; (d): deactivation; (i): activation; N/A: not available; SOZ: Seizure Onset Zone; IZ: Irritative Zone. BOLD: blood oxygen level-dependent signal; WC: wave_clus *: F contrast across all the IED classes. C: concordant; C+: concordant Plus; D: discordant; D+: discordant plus; N: null. GM: cluster of global maxima on fMRI maps. The black underlining shown the most clinically relevant IED classes related to both classification methods (see text for details).

IED in each case (IED1 for patients #4 and #7; IED2 for patient #8) and hemodynamic changes found within the brain lesion in three patients (75%). The other IED types were correlated with [N] results (IED2 for patients #4; IED 2 and 3 for patient #7; IED3 for patient #8) or discordant (IED3 and IED4 in #4, IED 1 in #8). For patient #2, the BOLD maps were classified as discordant plus [D+]. Interestingly, this patient is the only with poor surgery outcome (Class 5) and further surgery is planned.

With respect to the most clinically relevant IED types (Tables 1 and 3), there was a good correspondence between the GM-BOLD localization within IZ and the IED classification in two cases (50%): in patient #4, among the four IED types considered congruent with the IZ, only IED type 1 revealed [C] results. In patient #8, the fMRI map for IED type 2 was [C], and [D] for IED type 1. For patient #2, the BOLD map for the only visually labelled IED type (congruent with clinical hypothesis) was [D+]. Finally, in patient #7 the BOLD for IED type 1 (left temporal spikes) was found to be [C+].

GLM2. The BOLD global maximum related to one IED class (C1 for patients #2, #4, #7, #8) was located within the IZ (concordance classified as C or C+) in all patients (100%) and hemodynamic changes found within the brain lesion. The BOLD changes for the other IED types (C2–C3 for patients #4; C2–C4 for patient #7; C2–C3 for patient #8), [D+] (C3 in #2) or [N] (C2 in #2) were classed [D].

With respect to the IED types considered most clinically relevant, the BOLD map was classed as [C] or [C+] in 3/4 cases (75%): in patient #2, the only IED class considered congruent with the clinical hypothesis revealed a [C+] BOLD map; in patient #4, the BOLD map for only one IED class among the 3 considered to be clinically significant had a good degree of concordance [C+]; in patient #8, the only IED class considered congruent with the clinical hypothesis (C1) was associated with a concordant [C] BOLD map.

Comparison of interictal BOLD changes with the non-invasively defined (presumed) IZ

In the four cases (#1, #3, #5, #6) who did not undergo icEEG recordings, no structural abnormality was detected on MRI.

GLM1. The GM was located within the IZ in two cases (50%): in patient #3 both IED types 1 and 2 revealed concordant plus [C+] results; in

Please cite this article as: Pedreira, C., et al., Classification of EEG abnormalities in partial epilepsy with simultaneous EEG–fMRI recordings, NeuroImage (2014), http://dx.doi.org/10.1016/j.neuroimage.2014.05.009

patient #5, the fMRI maps obtained when IED types 1,2,3,4 were considered together were classified as concordant [C]. For both cases the other IED types did not show any significant BOLD cluster (classified as [N]). The maps were discordant [D] and discordant plus [D+] in patient #1 and discordant in patient #6.

Regarding the most clinically relevant IED types, there was good concordance in two patients (50%): in subject #3, both congruent IED types revealed [C+] findings; in patient #5, as previously observed, the four clinically significant IED types were associated with concordant [C] fMRI maps when considered together (F contrast across the four sets of regressors). Finally, for patient #1 and #6, the maps were discordant [D] for each of the most clinically relevant IED types (one per patient).

GLM2. The BOLD maps had a good degree of concordance in three cases (75%): in patient #1, the C7-related BOLD map was classed as concordant [C]; for patient #5, classes C1 and C4 were associated with concordant [C] BOLD maps; finally in patient #6, the BOLD map associated with the C2 IED was classed as concordant plus [C+]. The remaining IED classes were associated with discordant plus [D+] (classes C1, C3–C4), discordant [D] (C1 in patient #1, C1 in patient #6), [D+] (C3 patient #1) or Null [N] (C2, C4, C5, C6 for patient #1; C2–C3 for patient #5) or null [N] (class C2) BOLD maps.

Regarding the most clinically meaningful IED types, the BOLD maps had a good degree of concordance in three of the patients (75%): in case #1 two IED classes (C2, C7) had topographic distribution concordant with the electro-clinical hypothesis and the associated BOLD maps were discordant [D] for C2 and concordant plus [C+] for C7. In patient #5 class C1 was associated with a concordant BOLD map. Finally for patient #6, C2 IED were associated with a concordant BOLD pattern. For patient #3, the low amplitude bilateral fronto-central spikes (C1) considered congruent with clinical hypothesis were associated with a discordant [D] BOLD map.

Comparison of the GLM1 and GLM2 BOLD results

In summary, 13/26 (50%) visual IED types were associated with one or more regions of significant BOLD signal increase or decrease. At least one cluster of significant BOLD signal increase was detected in every patient, although not for all IED types. No region of significant BOLD change was revealed for one (patients #4 and #8), two (#7) or three (#3 and #5) IED types. In addition, in one patient (#5) in whom 5 out of the 7 IED types had a similar distribution on the scalp, regions of significant BOLD signal changes were revealed only when an SPM{F} contrast across the first four IED types was used. For the Wave_clus IED classification results, 21/29 IED classes were associated with significant BOLD signal changes (72%, compared to the 50% of visual classification), corresponding to a substantial increase in sensitivity. In all the classes a significant BOLD signal change was revealed except for the following: for patient #1, IED classes C2, C4, C5 and C6; C2 for patients #2 and #3; C2 and C3 for patient #5.

In the cases #7 and #8, in whom the algorithm IED classification matched completely (see Supplementary Material S1) with the one provided by the expert, GLM1 and GLM2 revealed maps with similar degrees of concordance; GLM2 revealed the same BOLD clusters as GLM1, plus 3 additional clusters (Table 3).

In cases when the algorithmic process demonstrated more IED classes than visual labelling (patients #1, #2 and #6), the degree of concordance was greater for GLM2 than for GLM1. Specifically, the GLM2 maps revealed additional clusters than the GLM1 maps (C7 in patient #1 and C2 in #6) or were similar to the GLM1 result but with greater concordance (for C1 in patient #2). There was only one BOLD cluster revealed by GLM1 that was not revealed by GLM2: the right posterior cingulate BOLD signal decrease related to IED2 in patient #1.

In cases when the algorithmic clustering identified fewer IED classes than the expert (patients #3, #4 and #5), the GLM2 and GLM1 were similarly concordant [C or C+] in two (#4 and #5). In these two cases, no BOLD clusters were lost. Furthermore, four additional clusters were revealed by GLM2 in patient #4 (see Table 3). In patient #3, in whom the algorithmic labelling failed to recognize as independent the right frontal, right temporal and left frontal IED, the GLM2 maps were classified as [D] in contrast to the GLM1 results. However, no BOLD clusters were lost and five additional clusters were revealed by GLM2 (see Table 3).

Representative examples

In the following, we present five particular cases to illustrate the characteristics of the algorithmic sorting. The cases presented represent two outcomes where the algorithm provides a better outcome (cases #1 and #6), one case in whom the two classification approaches revealed overlapping results, although with different SPM contrasts (case #5), the case where the reached solution did not match the expert solution and the outcome was not satisfactory in general terms (case #3) and finally one patient in whom the visual and the algorithm solutions gave similar findings in term of BOLD changes (cases #8). The results for the other cases are described and illustrated in the Supplementary Material (Supplementary Material S2, Supplementary Figs. 3, 4, 5).

Case 1 (Fig. 2)

Clinical background. Patient with pharmaco-resistant focal epilepsy, probably arising from the right temporal lobe. Video telemetry showed independent right fronto-temporal and mid-temporal spikes, left temporal spikes as well as bilateral spike-and-wave discharges. In the majority of seizures recorded, the EEG demonstrated fast waves and then epileptic discharges in right temporal regions (mid-temporal and posterior) followed by rapid spread over the left temporal cortex. Ictal semiology pointed towards a right neocortical origin. Nevertheless, this pattern was not consistent through the time and a more mesial origin with rapid spread over the neo-cortex wasn't excluded as well as a multifocal epileptogenic zone with the involvement of the left mesial temporal hemisphere. In term of IZ localization, the presence of two asynchronous IED types, the absence of MRI lesion and the not definitive localization of the SOZ did not allowed to exclude a complex interictal network, even multifocal. An interictal PET study showed left and right sided abnormalities, however the right temporo-parietal hypometabolism was the most prominent; a multifocal IZ (involving the right and the left temporal cortex) was suspected and the patient did not undergo intracranial recordings or surgery.

IED classification. The expert visually identified two IED types: right (N = 468) and left (N = 666) temporal spikes (Fig. 2A). The algorithmic sorting identified 7 IED classes (Fig. 2C): 3 with mostly left temporal localisation and which were differentiated by either amplitude [class #1 (N = 390; shown in blue in Fig. 2C) and class #3 (N = 127; green)] or the involvement of the right fronto-temporal region for class #5 (N = 84; magenta). Classes #2 and #7 consisted of right temporal spikes (N = 210; red and N = 89; grey). Class #6 consisted of high amplitude bilateral fronto-temporal spikes with emphasis on the left (N = 85; yellow). Class #4 consisted of very low amplitude bilateral occipital slow waves (N = 149; cyan). See Supplementary Material S1 for a quantification of the level of agreement between the two methods of IED classification.

EEG–fMRI results. The GLM1 maps corresponding to the two IED types were classified as discordant plus [D+] for the left IED and discordant [D] for the right IED. The left temporal IEDs were associated with a region of BOLD increase in the left temporal pole and decrease in the mid-posterior temporal lobe (GM) (Fig. 2B). The right temporal events were associated with a region of decrease in the right posterior cingulate (GM) (Fig. 2B).

GLM2 revealed BOLD signal changes over the right SMA (GM; increase) and the right superior frontal gyrus (clusters corresponding

UNCORRECTED PROOF

Please cite this article as: Pedreira, C., et al., Classification of EEG abnormalities in partial epilepsy with simultaneous EEG–fMRI recordings, NeuroImage (2014), http://dx.doi.org/10.1016/j.neuroimage.2014.05.009

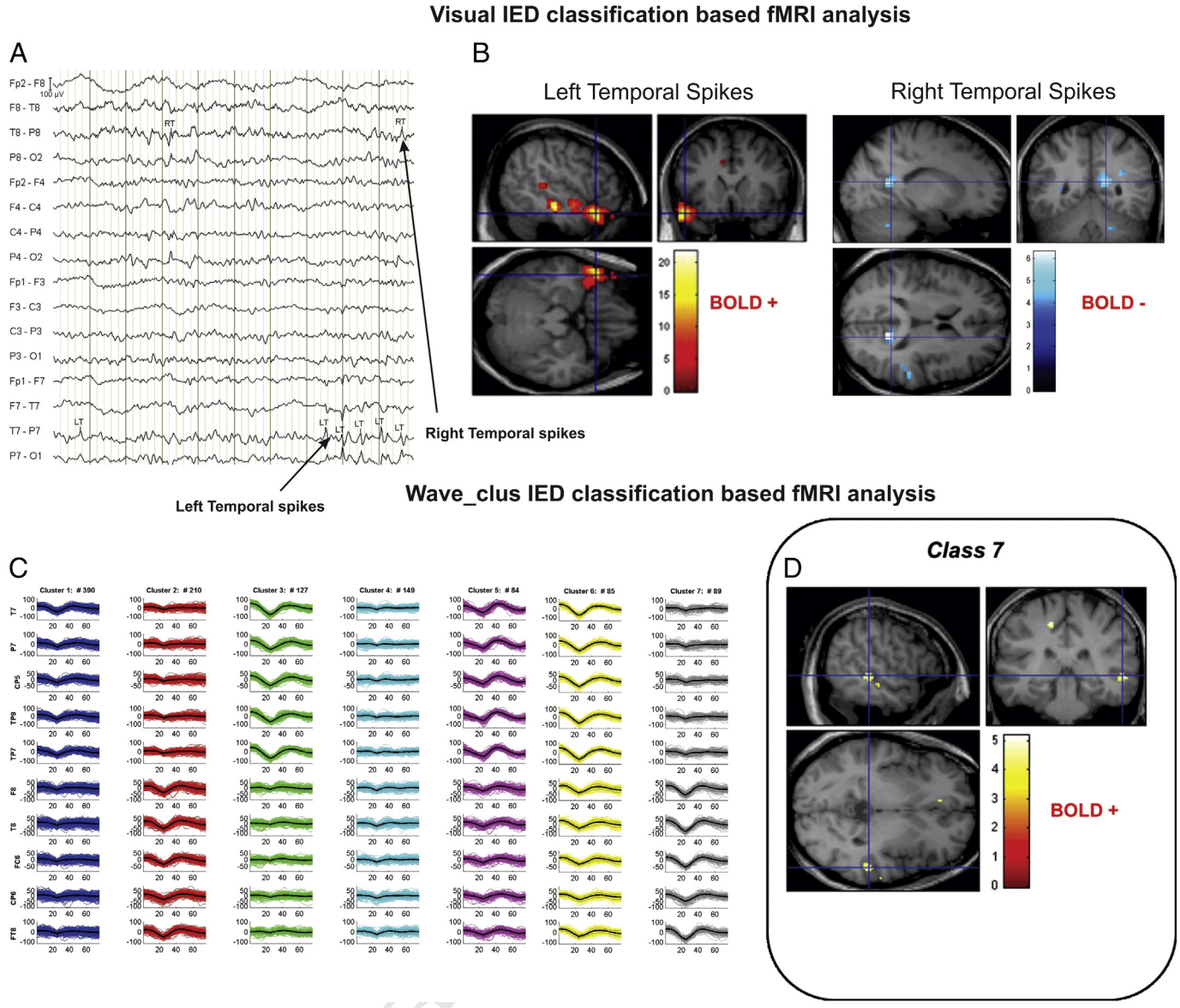

Fig. 2. Visual and algorithmic classification for the IED of case #1. The top of the figure (Panel A) presents the result of the classification of the IEDs according to the visual classification performed by the expert. The EEG was recorded during scanning after scanning and pulse artefact subtraction. The EEG trace is displayed as bipolar montage (64 channels). Two main classes of IED were marked: LT = Left Temporal Spikes; RT = Right Temporal Spikes. Panel B: EEG–fMRI data analysis results based on visual-IED labelling (T contrast, $p < 0.001$ uncorrected). See text for a detailed description of the IED-related BOLD changes. Panel C shows the 7 classes identified by the algorithmic solution. On the right hand side (Panel D) the result of the EEG–fMRI data analysis (T contrast, $p < 0.001$ uncorrected) associated to the class7 are displayed: a right middle temporal gyrus (BA22) BOLD signal increase is noted (crosshairs at the GM). All the fMRI results are overlaid on the subject's T1 image. BA: Brodmann Area. R = right; L = Left.

to increase and decrease) associated with the low amplitude left fronto-temporal spikes (C1); high amplitude left fronto-centro-temporal events (C3) were associated with a left temporal pole region of BOLD increase and a left mid-posterior temporal lobe region (GM) of decrease; high amplitude right fronto-centro-temporal spikes (C7) were associated with a global maximum cluster in the right middle temporal gyrus increase (region BA22; Fig. 2D). No significant clusters were found for C2, C4, C5 and C6 (hence classified as [N]). The degree of BOLD concordance was [C] for C7, [D] for C1 and [D+] for C3. Supplementary Fig. 2 shows the GLM2 results related to all IED classes. In summary, for patient #1 the algorithmic solution revealed a cluster of BOLD signal increase in the right temporal lobe probably representing the correct IZ, not previously observed.

Case 3 (Fig. 3)

Clinical background. Patient with right frontal lobe epilepsy. Interictal EEG showed diffuse Spike-Wave discharges with anterior and right predominance. Sleep is associated with increased IED occurrence. Left temporal IEDs were also recorded. Ictally, the EEG demonstrated a right frontal seizure onset in keeping with semiology. Based on the available electro-clinical data the presumed SOZ was located in the right frontal lobe; the IZ was less well localized, involving the right frontal area.

IED classification. The expert visually identified 5 classes: bifrontal (N = 253), right frontal (N = 71), left temporal (N = 21), left frontal (N = 18) and right temporal (N = 2) spikes (Fig. 3A). The algorithmic

Please cite this article as: Pedreira, C., et al., Classification of EEG abnormalities in partial epilepsy with simultaneous EEG–fMRI recordings, NeuroImage (2014), http://dx.doi.org/10.1016/j.neuroimage.2014.05.009

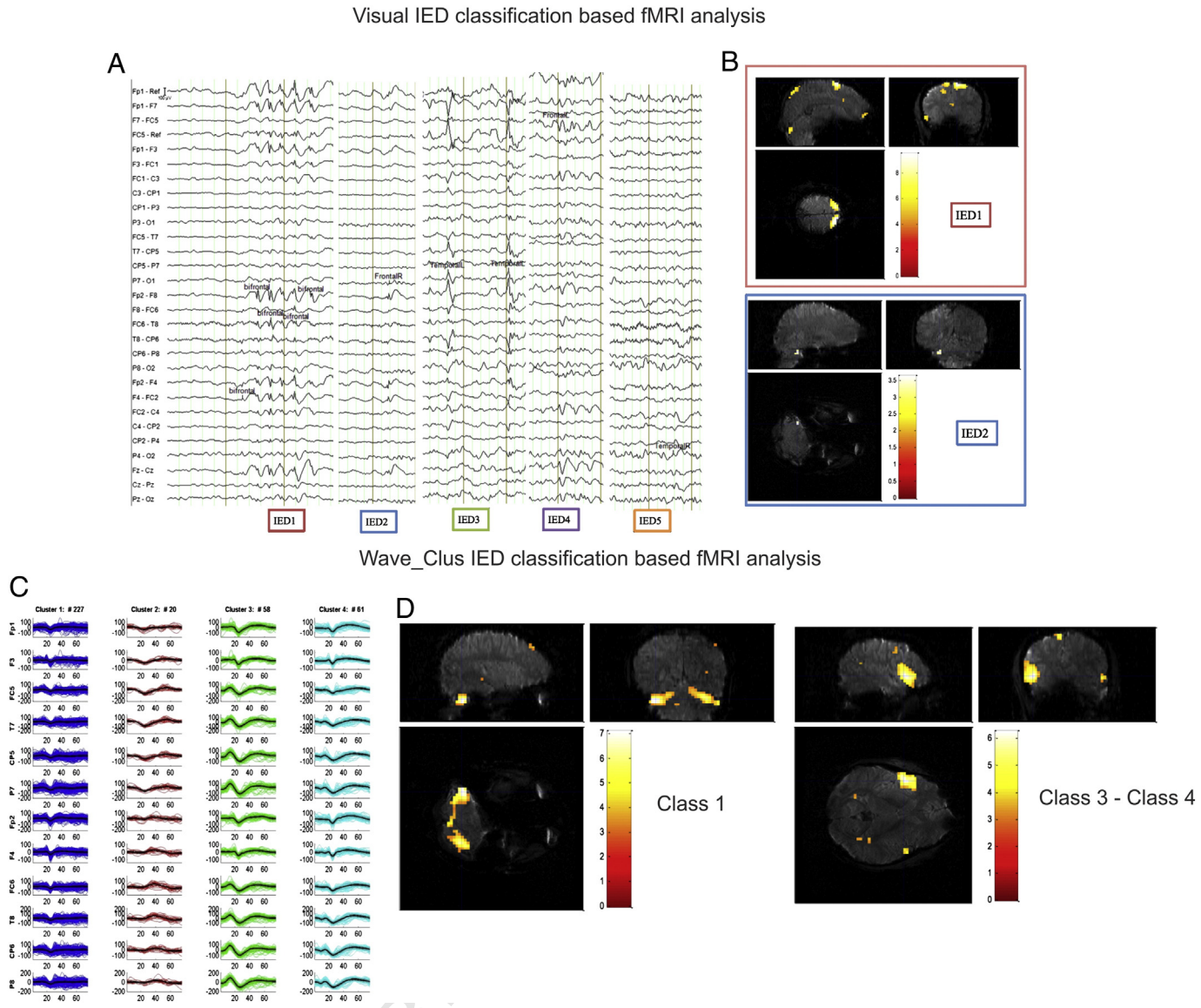

Fig. 3. Visual and algorithmic classification for the IED of case #3. The top of the figure (Panel A) presents the result of the classification of the IEDs according to the visual classification performed by the expert. The EEG was recorded during scanning after scanning artefact subtraction. The EEG trace is displayed as bipolar montage (32 channels). Five main classes of IED were marked (see main text for details). Panel B: EEG–fMRI data analysis results based on visual-IED labelling (T contrast, $p < 0.001$ uncorrected): BOLD increases were observed in the bilateral (more right) superior frontal gyrus (crosshairs at the GM) and left perisylvian cortex related to bifrontal IEDs while a widespread posterior BOLD decrease was observed covering the posterior DMN (data not shown). Right frontal Spikes were related to left cerebellum BOLD changes as increase; no hemodynamic decreases were detected. Left frontal, temporal and right temporal IEDs were not associated with significant BOLD changes. Panel C shows the 4 classes identified by the algorithmic solution. Panel D displayed the result of the EEG–fMRI data analysis associated to the *Wave_clus* IED classification algorithm (T contrast, $p < 0.001$ uncorrected): regions of significant BOLD change as increases were observed in the right left cerebellum (crosshairs at the GM), bilateral right superior frontal gyrus and left posterior temporal cortex associated with C1 events; C3 and C4 events correlated with a bilateral (more left) perisylvian cortex (crosshairs at the GM), left medial frontal gyrus, left precentral gyrus and right precuneus activations. A cluster of BOLD decrease was revealed over the left perisylvian cortex and right cerebellum for IED-C1 (data not shown). All the fMRI results are overlaid on the subject's high resolution T1 image. R = right; L = Left.

solution identified four classes, one corresponding to bilateral frontal events (C1, N = 227), one to the left fronto-temporal IED (C2; N = 21), one to high amplitude diffuse events (more centro-temporal) (C3; N = 56] and the last to low amplitude diffuse events (C4; N = 61) (Fig. 3C). We classified the level of agreement between the visual and the algorithmic classification as PM – (Supplementary Material S1).

EEG–fMRI results. GLM1 revealed a region of BOLD increase in the bilateral (more right) superior frontal gyrus (GM) related to the bifrontal IEDs (Fig. 3B). A cluster of activation over the left perisylvian cortex was also detected. Widespread posterior BOLD decrease covering the posterior part of the DMN was observed linked to the bifrontal IEDs. Right frontal Spikes were related to a left cerebellum BOLD changes as increase; no hemodynamic decreases were detected (Fig. 3B). The degree of BOLD concordance was [C+] for IED type1 (Bifrontal spikes) and [D] for IED type 2 (R frontal spikes). Left frontal, temporal and right temporal IEDs were not associated with significant BOLD changes (hence classified as [N]).

GLM2 revealed regions of significant BOLD change as increases in the left cerebellum (GM), right superior frontal gyrus and left posterior temporal cortex associated with low amplitude bilateral fronto-central spikes (C1); diffuse high amplitude (C3) and low amplitude (C4) events correlated with a bilateral (more left) perisylvian cortex (GM), left medial frontal gyrus, left precentral gyrus and right precuneus activations (Fig. 3D). A cluster of BOLD decrease was revealed over the left perisylvian cortex and right cerebellum for IED-C1 (data not shown). The level of concordance was [D+] for all of these IED classes. Finally, low amplitude left fronto-temporal events (C2) did not show any

Please cite this article as: Pedreira, C., et al., Classification of EEG abnormalities in partial epilepsy with simultaneous EEG–fMRI recordings, NeuroImage (2014), http://dx.doi.org/10.1016/j.neuroimage.2014.05.009

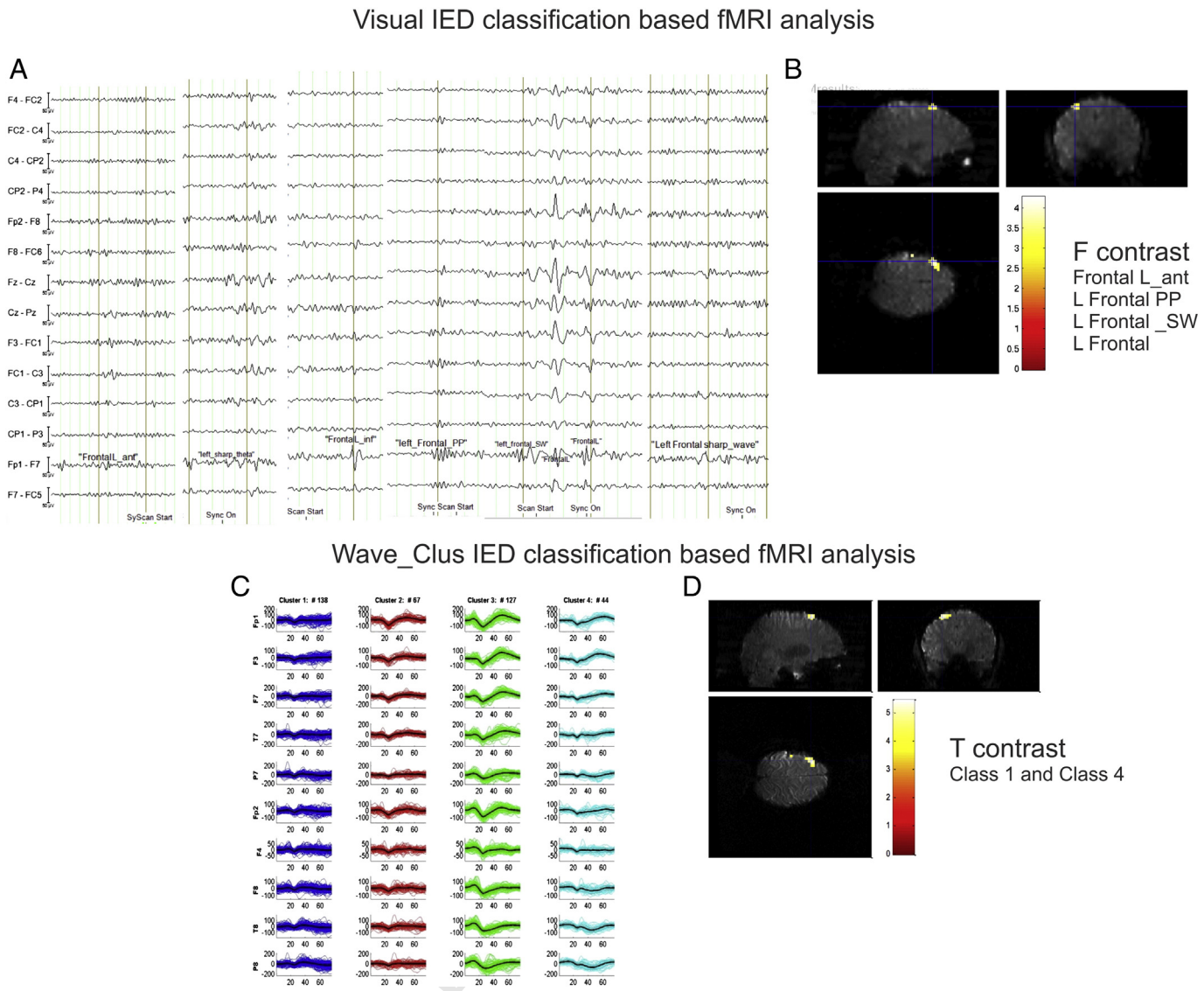

Fig. 4. Visual and algorithmic classification for the IED of case #5. Panel A presents the result of the classification of the IEDs according to the visual classification. The EEG was recorded during scanning after scanning artefact and pulse artefact subtraction. The EEG trace is displayed as bipolar montage (32 channels). Visual IED labelled 7 types of IED as described in the main text. Panel B: EEG–fMRI data analysis results based on visual-IED labelling (T contrast, $p < 0.001$ uncorrected): an increase in BOLD signal over the left superior frontal gyrus (crosshairs at the GM) was detected by means of an F contrast across the IED1, IED2, IED3 and IED4. Panel C shows the IED classification result as performed by the algorithm: four clusters of events were detected (see text for details). Panel D displayed the result of the EEG–fMRI data analysis based on the *Wave_clus* IED classification (T contrast, $p < 0.001$ uncorrected): a focal activation over the left superior frontal gyrus (GM) correlated with C1 and C4 independently (crosshairs at the GM). All the fMRI results are overlaid on the subject's high resolution T1 image. R = right; L = left.

significant increase or decrease in BOLD signal [N]. The patient is due to undergo intracranial EEG recordings.

This case represents the example in which the algorithms did not lead to concurrent results with the clinical evidence, resulting in fewer BOLD clusters than the visual inspection method and a lower degree of concordance based on the available non-invasive clinical evidence.

Case 5 (Fig. 4)

Clinical background. Patient with left frontal lobe epilepsy. EEG showed left frontal IEDs and bilateral SWD with left predominance. Ictally the EEG showed left theta activity and SWD over bilateral frontal regions. Based on the available electro-clinical data a left frontal cortex SOZ and IZ was hypothesized.

IED classification. Visual IED labelled 7 types of IED as left frontal spikes (IED1-N = 114), left frontal sharp-wave (IED2-N = 74), left frontal poly-spikes (IED3-N = 64), left frontal anterior spikes (IED4-N = 60), left frontal inferior spikes (IED5-N = 38), left frontal spike-wave (IED6-N = 19) and left frontal sharp theta activity (IED7-N = 3) (Fig. 4A). The algorithmic solution identified four IED classes, one corresponded to low amplitude diffuse events [C1-N = 138], one to low amplitude bilateral frontal events, more left [C2-N = 67], one to high amplitude diffuse (more frontal) IED [C3-N = 127] and the last to low amplitude left frontal spikes [C4-N = 44] (Fig. 4C). We classified the level of agreement between the visual and algorithmic classification as PM-.

EEG–fMRI results. Visually identified IED-based EEG–fMRI analysis demonstrated an increase in BOLD signal over the left superior frontal gyrus (GM) only when IED1, IED2, IED3 and IED4 were merged together with {F} contrast (Fig. 4B) classed as concordant [C]. IED5 to IED7 were not associated with significant BOLD signal changes [N].

The algorithmic EEG–fMRI analysis for C1 and C4 showed a focal activation (GM) over the left superior frontal gyrus (Fig. 4D). The level of concordance was assessed as [C] for both IED classes. C2 and C3

Please cite this article as: Pedreira, C., et al., Classification of EEG abnormalities in partial epilepsy with simultaneous EEG–fMRI recordings, NeuroImage (2014), http://dx.doi.org/10.1016/j.neuroimage.2014.05.009

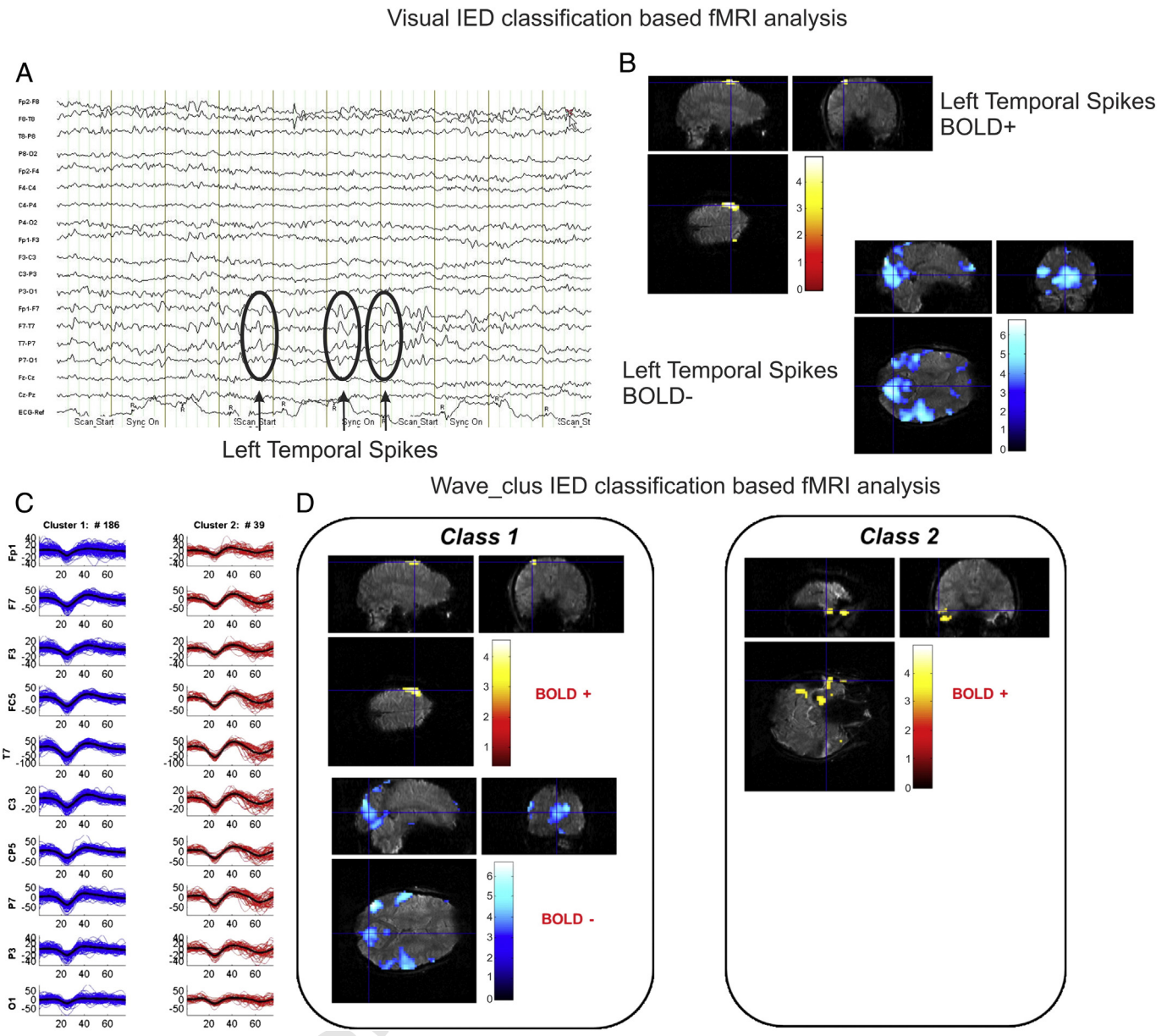

Fig. 5. Visual and algorithmic classification for the IED of case #6. The top of the figure (Panel A) presents results for the visual classification. EEG recorded during scanning after scanning artefact subtraction. The EEG trace was analysed following pulse (marked by R) and image artefact subtraction; the EEG trace is displayed as bipolar montage (32 channels). Note the presence of IED over left fronto-temporal regions. Panel B: EEG–fMRI data analysis results based on visual-IED labelling (T contrast, $p < 0.001$ uncorrected): an increase in the BOLD signal was found in the left precentral cortex and a decrease was seen over bilateral temporal lobes and the precuneus. Panel C shows the results of algorithmic labelling: 2 main classes were detected based on IED amplitude. Panel D: EEG–fMRI data analysis results based on algorithmic labelling: Class1 mapped over similar areas as the class from the visual classification did. Class2 was associated with a previously unseen activation in left temporal pole and posterior temporal lobe. No deactivation clusters were observed associated to Class2. All the fMRI results are overlaid on the subject's high resolution T1 image. R = right; L = left.

were not associated with significant BOLD changes [N]. The patient declined icEEG recording.

Case 6 (Fig. 5)

Clinical background. Patient with left temporal lobe epilepsy. The interictal EEG showed left temporal lobe IEDs; ictally, the EEG demonstrated rhythmic theta activity over the left temporal lobe. Based on the available electro-clinical information both SOZ and IZ are located over the left temporal lobe.

IED classification. The expert classified all events (225) as left temporal spikes (Fig. 5A). The algorithmic process identified two IED classes (Fig. 5C), one corresponding to high amplitude left spikes, mainly temporal (C1; N = 186, shown in blue in Fig. 3C), and another one to medium amplitude left IED, prevalent over the centro-temporal regions (C2; N = 39; shown in red).

EEG–fMRI results. GLM1 revealed a cluster of BOLD increase located in the left precentral cortex (BA6), and a decrease bilaterally in the temporal lobes and precuneus (GM) (Fig. 5B) corresponding to a level of concordance classed as [D].

The algorithmic EEG–fMRI data analysis (GLM2) showed a BOLD signal increase in the left precentral cortex (BA6) (GM) and widespread BOLD decreases over bilateral temporal lobes and precuneus associated with high amplitude diffuse left events (C1) (Fig. 5D). The events

Please cite this article as: Pedreira, C., et al., Classification of EEG abnormalities in partial epilepsy with simultaneous EEG–fMRI recordings, NeuroImage (2014), http://dx.doi.org/10.1016/j.neuroimage.2014.05.009

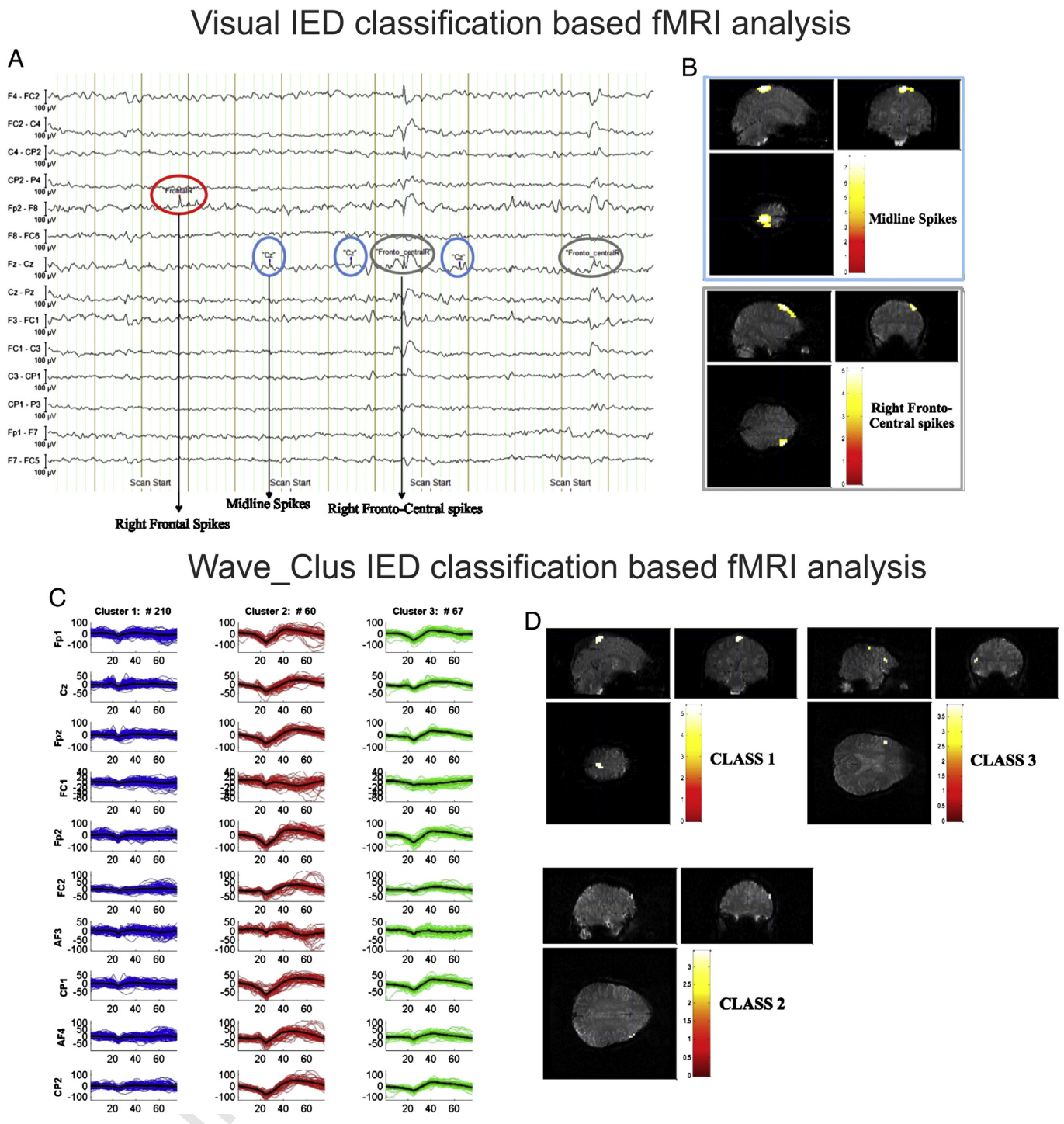

Fig. 6. Visual and algorithmic classification for the IED of case #8. The top of the figure (Panel A) presents results for the visual classification. EEG recorded during scanning after scanning artefact subtraction. The EEG trace was analysed following pulse (marked by R) and image artefact subtraction; the EEG trace is displayed as bipolar montage (32 channels). Note the presence of different types of IED marked: Midline spikes (IED1) in blue, Right fronto-central spikes (IED2) in grey and right frontal spikes in red (IED3). Panel B: EEG–fMRI data analysis results based on visual-IED labelling (T contrast, $p < 0.001$ uncorrected, crosshairs at the global maxima). A right middle frontal gyrus (BA9) activation (GM) corresponded to the IED1. IED2 led to a BOLD signal increase over the right medial frontal gyrus (BA6) (GM), while no hemodynamic changes were found related with the IED3 (Fig. 6B). Panel C: IED classification as result of the algorithm labelling: 3 IED classes were detected (see text for details). Panel D: EEG–fMRI data analysis results based on algorithmic labelling: Class1 identified a BOLD increase area on the right medial frontal gyrus (BA6) (GM), Class2 on the right middle frontal gyrus (BA9) (GM) to C2 and finally C3 demonstrate a left prefrontal cortex activation blob (BA10) (GM) (Fig. 6D). No deactivation clusters were observed associated to any Class. All fMRI results are overlaid subject's high resolution T1 image. R = right; BA: Brodmann area.

marked as medium amplitude left hemisphere IED (C2) were associated with a region of BOLD signal increase covering the pole and posterior parts of the left temporal lobe (GM) classed as [C+] (Fig. 5D). The C1-related map was classed as discordant [D]. The patient refused to undergo icEEG recordings.

Case 8 (Fig. 6)

Clinical background. Patient affected by right parietal lobe epilepsy symptomatic of right parietal FCD. Interictal EEG showed right parietal and right central IEDs. Ictal EEG demonstrated a continuous pattern of

Please cite this article as: Pedreira, C., et al., Classification of EEG abnormalities in partial epilepsy with simultaneous EEG–fMRI recordings, NeuroImage (2014), http://dx.doi.org/10.1016/j.neuroimage.2014.05.009

ARTICLE IN PRESS

right fronto-central spikes. Seizures' semiology revealed a sensitive aura (left leg paraesthesia) followed by left foot clonus which might continue for many hours and shown correlation with the spikes revealed by scalp EEG. A diffusion of the clonic jerks to the left leg and superior arm has been documented. An interictal PET scan demonstrated a moderate hypo-metabolism at the right fronto-polar and orbito-ventral cortex while an ictal SPECT seem to reveal an hypo-perfusion at the right temporal pole. The available non-invasive investigations, although suggested a SOZ in the right fronto-central cortex and the patient underwent icEEG recordings, showing a right pericentral cortex SOZ and the patient underwent resective surgery; The outcome at 5 months is ILAE Class1.

IED classification. Visual IED labelled three types of IED as midline central (IED1-N = 206), right fronto-central (IED2-N = 121) and right frontal spikes (IED3-N = 10) (Fig. 6A). The algorithmic solution identified three classes, one corresponded to low amplitude bilateral fronto-centro-parietal events [C1-N = 210], one to high amplitude bilateral fronto-centro-parietal IED [C2-N = 60] and finally one to low amplitude bilateral (>right) frontal spikes [C3-N = 67].

EEG–fMRI results. The visual EEG–fMRI data analysis for IED1 revealed a right middle frontal gyrus (BA9) activation (GM), classed as [D]. IED2 were associated with a region of BOLD signal over the right medial frontal gyrus (BA6) (GM) classed as [C]; for IED3 the result was [N] (Fig. 6B).

The automatic approach identified an area of BOLD increase in the right medial frontal gyrus (BA6) (GM) associated with C1, in the right middle frontal gyrus (BA9) (GM) for C2 and C3 was associated with a left prefrontal cortex activation blob (BA10) (GM) (Fig. 6D). The level of concordance was [C] for C1 and [D] for C2 and C3.

This case represents an example where the two solutions (visual and algorithm IED classification approaches) provided similar results in term of fMRI mapping of the presumed IZ and hence demonstrated a good reliability of the *Wave_clus* method.

Discussion

We have presented here the use of an automated spike sorting algorithm (*Wave_clus*) for the classification of IED events recorded during simultaneous EEG–fMRI and evaluated it using a double-blind process. Our approach integrates tools of signal processing and statistics into the IED classification process. Data were collected from 8 patients with refractory partial epilepsy within a pre-surgical evaluation protocol. This allowed us to compare the results of IED classification with purely visual marking by an expert observer, and to use a second set of observations, namely BOLD changes correlated with the IED classes, to assess the localization of brain regions associated with the electrophysiological activity, providing an evaluation of the solution proposed.

The main findings of this study are: (1) the approach based on spike sorting of the signals provided a nearly fully-automated, and hence potentially more objective classification, of interictal events visually identified previous to the application of the algorithm. The results obtained were generally in good agreement with expert classification, being able to identify IED classes related to fMRI maps concordant with the presumed IZ in 87% of the cases studied. This observation represents a promising outcome of the proposed method and its potential clinical applications especially in long-term EEG monitoring or icEEG recordings when used in conjunction with an automatic IED event detector (LeVan and Gotman, 2008); (2) the classification algorithm-based fMRI analysis demonstrated BOLD signal changes related to the majority of IED classes that provided an improved performance compared to the visual IED classification-based GLM (72% versus 50%); (3) the IED-related fMRI maps obtained using the algorithm classification had the global maximum located within the presumed IZ (confirmed by icEEG in 4 patients) in a greater proportion of cases than those derived from the visually IED classification approach (7 versus 5 of the cases); (4) with respect to the most clinically relevant IED types, the algorithm based fMRI analysis demonstrated concordant results (namely C and C+) in 6 patients (75%) compared to the four cases (hence 50%) when the visual classification was adopted. In summary, the proposed method provides a characterization of the IED events into classes that presented associated BOLD maps more consistent with the available electro-clinical evidence for the studied cases. Hence, the results of our study provided evidence that the algorithm solution might represent a new and powerful way of analysing EEG–fMRI signals, to assess the localization of brain regions associated with the electrophysiological activity and its clinical correlates. Furthermore, since the classification of IEDs using *Wave_clus* has proven successful and validated with the fMRI results, it is possible to consider its application for other epileptic recordings such as long term monitoring of EEG signals (outside the limitations of the fMRI scanner) and intracranial EEG recordings.

Automated classification of IEDs

The accurate identification of the area responsible for IED generation (i.e. the IZ) is an important element of the management of patients with drug-resistant epilepsy considered for surgery, with improved outcome associated with removal of the IZ in cases with localized IED and concordant with the clinical information (Dworetzky and Reinsberger, 2011; Marsh et al., 2010). Additionally, human and animal studies raise the possibility that IEDs contribute to the development of the neuronal circuits that give rise to spontaneous seizures (Staley et al., 2005), although it has also been proposed that they could have a protective effect for the epileptic area (Curtis and Avanzini, 2001). The process of identifying the IZ rests on the accurate detection and classification of IED. In clinical practice, this can be a difficult undertaking particularly for patients with complex and varied abnormal EEG features and for prolonged EEG recordings which can last from a few to many days. For this reason, automatic spike and seizure detection and classification techniques have received intense attention (Yadav et al., 2011).

Sorting algorithms, based on the waveform of the recorded signals, have been applied to electrophysiological recordings from microelectrodes for the identification of neuronal source signals for decades (see Quian Quiroga, 2007 for a review). Recently, they have increased their performance taking advantage of multiple-site recordings and proving their contribution this complex recording scenario (Blanche et al., 2005; Gray et al., 1995). However, up to our knowledge, spike sorting algorithms for extracellular recordings have not previously been used for the classification of EEG-related signals. In here, we have shown that its use is not only possible, but desirable, in the classification of IEDs for the diagnosis of epilepsy.

The goal of our study was to provide a method of analysing the EEG signals of any given recording that would maximize the information extracted from the recorded IEDs while, at the same time, diminish the subjectivity of the present IEDs classification methods. In our work we only focused on maximizing the performance on the event classification and did not include an automatic detection as previous studies have done (Hogan, 2011; Hostetler et al., 1992).

In this study we assessed the validity of the approach by comparing the automated classification results to those obtained visually. We contrasted both the EEG events themselves and associated fMRI signal changes in a group of 8 patients for whom good, independent IZ localization information was available. Our results suggest that the proposed approach offers a valid classification and it is a promising complement to automated detection methodologies. Furthermore, the results obtained provided more classes related to the IZ than the manual classification. In addition, the use of algorithmic event classification could allow correction of false detections, as it is likely that they will be grouped in separate clusters. These clusters could be visually inspected and all the spurious events, such as eye blinks and head motions, grouped together by the algorithm in a cluster, could be rejected in one action. Others, such as inconsistent EEG events, would not elicit any associated fMRI

UNCORRECTED PROOF

Please cite this article as: Pedreira, C., et al., Classification of EEG abnormalities in partial epilepsy with simultaneous EEG–fMRI recordings, NeuroImage (2014), http://dx.doi.org/10.1016/j.neuroimage.2014.05.009

signal. Hence, the solution proposed showed a marked improvement compared to the visual solution reached by the individual classification of events from the user, despite the user's supervision of the proposed outcome before the final solution.

IED classification and localization

Our general approach to IED identification and classification for the purpose of fMRI modelling is based on the principle of building a complete and specific predictor of the fMRI signal changes. The predictor is built under a compromise to optimise sensitivity and specificity of the epilepsy-related BOLD changes while limiting the number of GLM tested to a single one. Hence, we build a single GLM that embodies our best hypothesis about the underlying sources of the fMRI signal variations and how they are reflected on EEG (Salek-Haddadi et al., 2006). Therefore, we tend to include as an effect of interest any event that may be associated with fMRI signal change, and try to separate effects that may be associated with different BOLD regions or networks.

The total number of IED classes across the group was similar: 26 for the visual classification compared to 29 for the algorithmic one. The two approaches demonstrated similar degrees of correspondence between the IED localization and the presumed or confirmed IZ (see the Supplementary Material for details) with 87% of IED classes concordant with the presumed or confirmed IZ. The most relevant question for our results would be: "Does the algorithmic result give more localizing information on the IZ than the visual classification?" Answering this question will require further investigation, such as prospective studies in a clinical context. Nonetheless, the fMRI element of our study provides some evidence relevant to the question.

In three cases (#1, #2 and #6) of the presented study the results with the automatic classification method reported a higher number of clusters, which in turn, led to fMRI maps more concordant to the clinical evidence than the ones reported for visual classification (see the results section and Table 3 for details).

In two further cases (#4 and #5) the labelling obtained for both methods differed in the type of classes obtained. While the expert reported classes based in morphology, the algorithmic method obtained more IED localization based classes. Nonetheless, the fMRI maps related to both approaches in these two cases were in broad agreement and concordant with the IZ. These results pose an interesting question about the possibility of overclustering risks in visual classification (especially in case #5, in which the merging of visual classes led to activation maps in the fMRI signal), as we would expect correctly classified IED to be associated with greater BOLD sensitivity (Flanagan et al., 2009). Interestingly, even in a case in which the number of clusters was lower for the automatic classification (#3), covering only partially the topographic distribution of the visually-labelled IED (see Supplementary Material), both approaches revealed clinically-relevant IED and the related BOLD maps included almost the same clusters, although the location of the global maxima (and hence the level of concordance) was different.

Regarding the clinical significance of the IED classification, in the Supplementary Material we have distinguished between potentially meaningful IED types from others. Although this distinction can be seen as arbitrary, especially in those cases without icEEG recordings, we believe that it is relevant for the interpretation of the results obtained with the proposed solution and its clinical utility. The results obtained for both approaches also differed for the non-congruent classes. According to the preponderant clinical hypotheses, visual classification revealed 8 IED classes (38%) that were judged incongruent across the entire group of patients compared to 16 (55%) for the algorithmic solution. However, the fMRI maps associated to the two types of analysis were different. While all visually classified incongruent IEDs resulted in BOLD activity maps classified as discordant or NULL (except for patient #7 and for the type IED1 of patient #1), the algorithmic classification presented a mixed type of BOLD maps for incongruent IEDs. In the later case, the total number of classes accounting for discordant or NULL classification was only of 10 of the 16 classes while the other 6 presented some relationship with the epileptogenic network. This may indicate that the automated classifier could be providing some additional information. In order to assess this, more analysis would be needed to study the clinical relevance of this type of activations.

Algorithmic sensitivity and specificity

fMRI mapping failed to reveal significant hemodynamic changes in relation to 50% of IED-types for the visual classification compared to 28% for the algorithmic clustering. The relatively high proportion of NULL results, especially regarding the visual IED classification related fMRI analyses, is in line with previously reported observations. Different papers indeed reported a variable percentage between 30% and 70% of EEG–fMRI recordings in patients with focal epilepsy, that did not revealed any significant spike-related BOLD changes despite the presence of recorded events (Aghakhani et al., 2006; Grouiller et al., 2011; Salek-Haddadi et al., 2006; Storti et al., 2013). Within the group of IEDs with fMRI hemodynamic changes, the proportion of IED types with discordant fMRI maps was 27% and 38% for visual and algorithmic labelling, respectively. However, in the majority of patients the algorithmic-derived BOLD maps were more localizing the IZ (C and C + results) than the visual classification-derived ones. Improved concordance was observed in the patients for whom algorithmic labelling provided additional IED classes (cases #1, #2 and #6). It is notable that concordant fMRI maps were associated with clinically meaningful IED, suggesting that algorithmic solutions can provide more clinically relevant localizing information, improving sensitivity of EEG–fMRI co-registration in severe partial epilepsies.

Given the small population sample, it is difficult to assess specificity of algorithmic approach rigorously. In our centre and in many others, the icEEG is considered the gold standard to localize the IZ (Luders and Schuele, 2006; Rosenow and Luders, 2001) and when not available localization provided by non-invasive means is acceptable. It is important to keep in mind that the EEG–fMRI studies reveal often a network characterized by several clusters of BOLD changes so that the technique is not expected to specifically pinpoint the source of epileptic activity. Nevertheless, in the majority of our patients (7/8), the localization of the statistical maximum provided by the automatic IED classification was specifically concordant with the presumed target area.

Taken together, our findings suggest that the analysis of IEDs using automatic methods provides a high level of concordance between the associated fMRI clusters and the IZ of focal epilepsy, providing more significant clusters associated with the epileptic regions. In addition, the method, being almost fully automatic might offer a more objective evaluation of the recorded events.

Methodological considerations and future work

We used a less stringent statistical significance threshold than the conventional value used in most cognitive fMRI studies ($p < 0.001$ without correction for multiple comparisons). However, there are several evidences that have shown and evaluated the clinical value of uncorrected results, including findings within the pre-surgical assessment of drug-resistant epileptic patients. Indeed, a good concordance was detected between IED related BOLD changes ($p < 0.001$ uncorrected) with the IZ as defined by the intracranial recordings (Grouiller et al., 2011) and by the postsurgical outcome (Thornton et al., 2010). In a recent paper (Zijlmans et al., 2007), the uncorrected pre-surgical IED-related fMRI maps revealed BOLD clusters concordant with the epileptogenic zone in patients with drug-resistant epilepsies previously excluded from surgery for presumed multifocality. In our study the use of a less conservative threshold can be partly justified by the desire to extract as much information as possible from each dataset (given its potential clinical relevance for the individual patient's management),

UNCORRECTED PROOF

Please cite this article as: Pedreira, C., et al., Classification of EEG abnormalities in partial epilepsy with simultaneous EEG–fMRI recordings, NeuroImage (2014), http://dx.doi.org/10.1016/j.neuroimage.2014.05.009

ARTICLE IN PRESS

our use of extensive confound effect modelling strategies (Chaudhary et al., 2012; Liston et al., 2006; Salek-Haddadi et al., 2006; Thornton et al., 2010, 2011; Vulliemoz et al., 2011), and the usual existence of a prior localization hypothesis (Carney et al., 2012; Thornton et al., 2011). Furthermore, the application of an additional five voxels threshold was applied in order to discard BOLD changes occurring in scattered voxels. The results shown here are encouraging enough to warrant the application of the automated classification technique in a larger group of patients, and for the analysis of icEEG-fMRI data, which has abundance of IED (Carmichael et al., 2012; Vulliemoz et al., 2011).

In our study, we selected patients with very frequent IED to satisfy a requirement of the algorithm. Such datasets represent the greatest challenge for visual IED classification being laborious and time-consuming. Given the success of this study, the application of the proposed solution to interictal activity recorded intra-cranially might be fruitful (Yadav et al., 2011). Our findings support the idea that spike sorting algorithms adapted for multiple-site recordings, such as *Wave_clus*, could be the basis of a completely automatic solution for the classification of IED in long term and/or intracranial EEG recordings by combining it with an automatic detection algorithm (see Hostetler et al., 1992; Webber et al., 1993 for examples).

Conclusions

In this study we have presented the analysis of 8 cases of epileptic patients in which we have increased the clinically-relevant information extracted from their EEG–fMRI co-registration. We have demonstrated the successful application of an automated spike sorting algorithm in the classification of IEDs on scalp EEG recorded during fMRI. The results obtained showed that, by using this approach, we could detect a higher number of IED classes associated with BOLD changes, corresponding to an increase in EEG–fMRI sensitivity, which could not be explained by the mere increase in the number of total classes. In addition, the results show that the combination of algorithmic classification of IEDs with automatic event detection could form a clinically useful tool in the pre-surgical assessment of patients with severe epilepsy.

Supplementary data to this article can be found online at http://dx.doi.org/10.1016/j.neuroimage.2014.05.009.

Uncited references

Alarcon et al., 1997
Rémi et al., 2011
Zhang et al., 2012

References

Aghakhani, Y., Kobayashi, E., Bagshaw, A.P., Hawco, C., Benar, C.G., Dubeau, F., et al., 2006. Cortical and thalamic fMRI responses in partial epilepsy witfocal and bilateral synchronous spikes. Clin. Neurophysiol. 117, 177–191.

Alarcon, G., Garcia Seoane, J.J., Binnie, C.D., Martin Miguel, M.C., Juler, J., Polkey, C.E., Elwes, R.D., et al., 1997. Origin and propagation of interictal discharges in the acute electrocorticogram. Implications for pathophysiology and surgical treatment of temporal lobe epilepsy. Brain 120, 2259–2282.

Al-Asmi, A., Bènar, C.G., Gross, D.W., Khani, Y.A., Andermann, F., Pike, B., et al., 2003. fMRI activation in continuous and spike-triggered EEG–fMRI studies of epileptic spikes. Epilepsia 44, 1328–1339.

Allen, P.J., Polizzi, G., Krakow, K., Fish, D.R., Lemieux, L., 1998. Identification of EEG events in the MR scanner: the problem of pulse artifact and a method for its subtraction. Neuroimage 8, 229–239.

Allen, P.J., Josephs, O., Turner, R., 2000. A method for removing imaging artifact from continuous EEG recorded during functional MRI. Neuroimage 12, 230–239.

Blanche, T.J., Spacek, M.A., Hetke, J.F., Swindale, N.V., 2005. Polytrodes: high-density silicon electrode arrays for large-scale multiunit recording. J. Neurophysiol. 93, 2987–3000.

Carmichael, D.W., Vulliemoz, S., Rodionov, R., Thornton, J.S., McEvoy, A.W., Lemieux, L., 2012. Simultaneous intracranial EEG–fMRI in humans: protocol considerations and data quality. Neuroimage 63, 301–309.

Carney, P.W., Masterton, R.A., Flanagan, D., Berkovic, S.F., Jackson, G.D., 2012. The frontal lobe in absence epilepsy: EEG–fMRI findings. Neurology 78, 1157–1165.

Chaudhary, U.J., Carmichael, D.W., Rodionov, R., Thornton, R.C., Bartlett, P., Vulliemoz, S., et al., 2012. Mapping preictal and ictal hemodynamic networks using video-electroencephalography and functional imaging. Brain 135, 3645–3663.

Curtis, M., Avanzini, G., 2001. Interictal spikes in focal epileptogenesis. Prog. Neurobiol. 63, 541–567.

Dworetzky, B.A., Reinsberger, C., 2011. The role of the interictal EEG in selecting candidates for resective epilepsy surgery. Epilepsy Behav. 20, 167–171.

Ebersole, J.S., 1997. Defining epileptogenic foci: past, present, future. J. Clin. Neurophysiol. 14, 470.

Emerson, R.G., Pedley, T.A., 2000. Electroencephalography and evoked potentials. Neurol. Clin. Pract. 1, 473–485.

Flanagan, D., Abbott, D.F., Jackson, G.D., 2009. How wrong can we be? The effect of inaccurate mark-up of EEG–fMRI studies in epilepsy. Clin. Neurophysiol. 120 (9), 1637–1647.

Friston, K.J., Williams, S., Howard, R., Frackowiak, R.S., Turner, R., 1996. Movement-related effects in fMRI time-series. Magn. Reson. Med. 35, 346–355.

Gray, C.M., Malnonado, P.E., Wisoln, M., Mcnaughton, B., 1995. Tetrodes markedly improve the reliability and yield of multiple single-unit isolation from multi-unit recordings in cat striate cortex. J. Neurosci. Methods 63, 43–54.

Grouiller, F., Thornton, R.C., Groening, K., Spinelli, L., Duncan, J.S., Schaller, K., et al., 2011. With or without spikes: localization of focal epileptic activity by simultaneous electroencephalography and functional magnetic resonance imaging. Brain 134, 2867–2886.

Hamer, H.M., Morris, H.H., Mascha, E.J., Karafa, M.T., Bingaman, W.E., Bej, M.D., et al., 2002. Complications of invasive video-EEG monitoring with subdural grid electrodes. Neurology 58, 97–103.

Hogan, R.E., 2011. Automated EEG, detection algorithms and clinical semiology in epilepsy: importance of correlations. Epilepsy Behav. 22 (Suppl. 1), S4–S6 (Dec).

Hostetler, W.E., Doller, H.J., Homan, R.W., 1992. Assessment of a computer program to detect epileptiform spikes. Electroencephalogr. Clin. Neurophysiol. 83 (1), 1–11.

Lemieux, L., Salek-Haddadi, A., Lund, T.E., Laufs, H., Carmichael, D., 2007. Modelling large motion events in fMRI studies of patients with epilepsy. Magn. Reson. Imaging 25, 894–901.

LeVan, P., Gotman, J., 2008. Automatic detection of epileptic spikes. In: Lüders, H.O., Bongaman, W., Najm, I.M. (Eds.), Textbook of Epilepsy Surgery. Taylor & Francis, Abingdon, UK.

Liston, A.D., Lund, T.E., Salek-Haddadi, A., Hamandi, K., Friston, K.J., Lemieux, L., 2006. Modelling cardiac signal as a confound in EEG–fMRI and its application in focal epilepsy studies. Neuroimage 30, 827–834.

Luders, H., 1993. General principles. Surgical Treatment of the Epilepsies pp. 137–153.

Luders, H., Schuele, S.U., 2006. Epilepsy surgery in patients with malformations of cortical development. Curr. Opin. Neurol. 19 (2), 169–174.

Marsh, E.D., Peltzer, B., Brown III, M.W., Wusthoff, C., Storm Jr., P.B., Litt, B., et al., 2010. Interictal EEG spikes identify the region of electrographic seizure onset in some, but not all, pediatric epilepsy patients. Epilepsia 51, 592–601.

Mégevand, P., Spinelli, L., Genetti, M., Brodbeck, V., Momjian, S., Schaller, K., et al., 2013. Electric source imaging of interictal activity accurately localises the seizure onset zone. JNNP 30, 1–6.

Pittau, F., Dubeau, F., Gotman, J., 2012. Contribution of EEG–fMRI to the definition of the epileptic focus. Neurology 78, 1479–1487.

Quian Quiroga, R., 2007. Spike sorting. Scholarpedia 2, 3583.

Quian Quiroga, R., Nadasdy, Z., Ben-Shaul, Y., 2004. Unsupervised spike detection and sorting with wavelets and super-paramagnetic clustering. Neural Comput. 16, 1661–1687 (5).

Ramabhadran, B., Frost Jr., J.D., Glover, J.R., Ktonas, P.Y., 1999. An automated system for epileptogenic focus localization in the electroencephalogram. J. Clin. Neurophysiol. 16 (1), 59–68.

Rémi, J., Vollmar, C., de Marinis, A., Heinlin, J., Peraud, A., Noachtar, S., 2011. Congruence and discrepancy of interictal and ictal EEG with MRI lesions in focal epilepsies. Neurology 77, 1383–1390.

Rosenow, F., Luders, H., 2001. Presurgical evaluation of epilepsy. Brain 124, 1683–1700.

Salek-Haddadi, A., Diehl, B., Hamandi, K., Merschhemke, M., Liston, A., Friston, K., Duncan, J.S., Fish, D.R., Lemieux, L., 2006. Hemodynamic correlates of epileptiform discharges: an EEG–fMRI study of 63 patients with focal epilepsy. Brain Res. 1088, 148–166.

Scherg, M., Ille, N., Weckesser, D., Ebert, A., Ostendorf, A., Boppel, T., Schubert, S., et al., 2012. Fast evaluation of interictal spikes in long-term EEG by hyper-clustering. Epilepsia 53 (7), 1196–1204.

Siniatchkin, M., Moeller, F., Jacobs, J., Stephani, U., Boor, R., Wolff, S., et al., 2007. Spatial filters and automated spike detection based on brain topographies improve sensitivity of EEG–fMRI studies in focal epilepsy. Neuroimage 37 (3), 834–843.

Staley, K., Hellier, J.L., Dudek, F.E., 2005. Do interictal spikes drive epileptogenesis? Neuroscientist 11 (4), 272–276.

Staley, K.J., White, A., Dudek, F.E., 2011. Interictal spikes: harbingers or causes of epilepsy? Neurosci. Lett. 27, 247–250.

Storti, S.F., Formaggio, E., Bertoldo, A., Manganotti, P., Fiaschi, A., Toffolo, G.M., 2013. Modelling hemodynamic response function in epilepsy. Clin. Neurophysiol. 124, 2108–2118.

Thornton, R., Laufs, H., Rodionov, R., Cannadathu, S., Carmichael, D.W., Vulliemoz, S., et al., 2010. EEG correlated functional MRI and postoperative outcome in focal epilepsy. J. Neurol. Neurosurg. Psychiatry 81 (8), 922–927.

Thornton, R., Vulliemoz, S., Rodionov, R., Carmichael, D.W., Chaudhary, U.J., Diehl, B., et al., 2011. Epileptic networks in focal cortical dysplasia revealed using electroencephalography-functional magnetic resonance imaging. Ann. Neurol. 70 (5), 822–837.

UNCORRECTED PROOF

Please cite this article as: Pedreira, C., et al., Classification of EEG abnormalities in partial epilepsy with simultaneous EEG–fMRI recordings, NeuroImage (2014), http://dx.doi.org/10.1016/j.neuroimage.2014.05.009

ARTICLE IN PRESS

Vulliemoz, S., Carmichael, D.W., Rosenkranz, K., Diehl, B., Rodionov, R., Walker, M.C., et al., 2011. Simultaneous intracranial EEG and fMRI of interictal epileptic discharges in humans. Neuroimage 54, 182–190.
Webber, W.R., Litt, B., Lesser, R.P., Fischer, R.S., Bankman, I., 1993. Automatic EEG spike detection: what should the computer imitate? Electroencephalogr. Clin. Neurophysiol. 87 (6), 364–367.
White, A., Williams, P.A., Hellier, J.L., Clark, S., Edward, D.F., Staley, K.J., 2010. EEG spike activity precedes epilepsy after kainate-induced status epilepticus. Epilepsia 51 (3), 371–383.
Yadav, R., Shah, A.K., Loeb, J.A., Swamy, M.N., Agarwal, R., 2011. A novel unsupervised spike sorting algorithm for intracranial EEG. Conf. Proc. IEEE Eng. Med. Biol. Soc. 2011, 7545–7548.
Zhang, J., Liu, W., Chen, H., Xia, H., Zhou, Z., Wang, L., et al., 2012. EEG–fMRI validation studies in comparison with icEEG: a review. Int. J. Psychophysiol. 84, 233–239.
Zijlmans, M., Huiskamp, G., Hersevoort, M., Seppenwoolde, J.H., van Huffelen, A.C., Leijten, F.S., 2007. EEG–fMRI in the preoperative work-up for epilepsy surgery. Brain 130, 2343–2353.

UNCORRECTED PROOF

Please cite this article as: Pedreira, C., et al., Classification of EEG abnormalities in partial epilepsy with simultaneous EEG–fMRI recordings, NeuroImage (2014), http://dx.doi.org/10.1016/j.neuroimage.2014.05.009